

AD-A255 165



2

# NAVAL POSTGRADUATE SCHOOL Monterey, California



**S** DTIC  
ELECTE  
SEP 15 1992  
**A** **D**

## THESIS

STUDY OF SOUND PROPAGATION  
IN A WEDGE-SHAPED OCEAN AND COMPARISON  
WITH OTHER METHODS

by

George Nassopoulos

June, 1992

Advisor:

Alan B. Coppins

Approved for public release; distribution is unlimited.

92-25145



92 9 14 039

REPORT DOCUMENTATION PAGE			
1a. REPORT SECURITY CLASSIFICATION UNCLASSIFIED		1b. RESTRICTIVE MARKINGS	
2a. SECURITY CLASSIFICATION AUTHORITY		3. DISTRIBUTION/AVAILABILITY OF REPORT Approved for public release; distribution is unlimited.	
2b. DECLASSIFICATION/DOWNGRADING SCHEDULE			
4. PERFORMING ORGANIZATION REPORT NUMBER(S)		5. MONITORING ORGANIZATION REPORT NUMBER(S)	
6a. NAME OF PERFORMING ORGANIZATION Naval Postgraduate School	6b. OFFICE SYMBOL (If applicable) 52	7a. NAME OF MONITORING ORGANIZATION Naval Postgraduate School	
6c. ADDRESS (City, State, and ZIP Code) Monterey, CA 93943-5000		7b. ADDRESS (City, State, and ZIP Code) Monterey, CA 93943-5000	
8a. NAME OF FUNDING/SPONSORING ORGANIZATION	8b. OFFICE SYMBOL (If applicable)	9. PROCUREMENT INSTRUMENT IDENTIFICATION NUMBER	
8c. ADDRESS (City, State, and ZIP Code)		10. SOURCE OF FUNDING NUMBERS	
		Program Element No	Project No
		Task No	Work Unit Accession Number
11. TITLE (Include Security Classification) STUDY OF SOUND PROPAGATION IN A WEDGE-SHAPED OCEAN AND COMPARISON WITH OTHER METHODS			
12. PERSONAL AUTHOR(S) NASSOPOULOS, GEORGE			
13a. TYPE OF REPORT Master's Thesis	13b. TIME COVERED From To	14. DATE OF REPORT (year, month, day) 1992 June	15. PAGE COUNT 88
16. SUPPLEMENTARY NOTATION The views expressed in this thesis are those of the author and do not reflect the official policy or position of the Department of Defense or the U.S. Government.			
17. COSATI CODES		18. SUBJECT TERMS (continue on reverse if necessary and identify by block number)	
FIELD	GROUP	SUBGROUP	
		Wedge-shaped ocean	
19. ABSTRACT (continue on reverse if necessary and identify by block number) After several years of research, the image theory has been found acceptable to solve the sound propagation problem within a wedge-shaped fluid overlying either a slow or a fast bottom. Some further observations were done in this research. The primary purpose was the development and computer application of a new analysis, the doublet analysis, based on the image theory. In this analysis, the features of the image theory are studied from another point of view, based on a collection of acoustic doublets.			
20. DISTRIBUTION/AVAILABILITY OF ABSTRACT <input checked="" type="checkbox"/> UNCLASSIFIED/UNLIMITED <input type="checkbox"/> SAME AS REPORT <input type="checkbox"/> DTIC USERS		21. ABSTRACT SECURITY CLASSIFICATION UNCLASSIFIED	
22a. NAME OF RESPONSIBLE INDIVIDUAL Alan B. Coppens		22b. TELEPHONE (Include Area code) (408) 646-2116	22c. OFFICE SYMBOL PH/Cz

Approved for public release; distribution is unlimited.

**Study of Sound Propagation in a  
Wedge-shaped Ocean and Comparison  
with Other Methods**

by

George Nassopoulos  
Lieutenant J.G., Hellenic Navy  
B.S., Hellenic Naval Academy, 1983

Submitted in partial fulfillment  
of the requirements for the degree of

MASTER OF SCIENCE IN ENGINEERING ACOUSTICS

from the

NAVAL POSTGRADUATE SCHOOL


June 1992

Author:

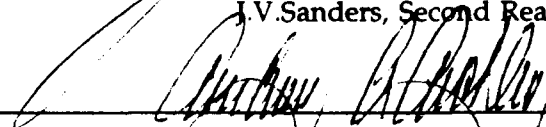


George Nassopoulos

Approved by:

  
A.B. Coppens, Thesis Advisor

J.V. Sanders, Second Reader



A. Atchley, Chairman

Engineering Acoustics Academic Group

### ABSTRACT

After several years of research, the image theory has been found acceptable to solve the sound propagation problem within a wedge-shaped fluid overlying either a slow or a fast bottom. Some further observations were done in this research. The primary purpose was the development and computer application of a new analysis, the doublet analysis, based on the image theory. In this analysis, the features of the image theory are studied from another point of view, based on a collection of acoustic doublets.

Accession For	
NTIS CRA&I	<input checked="" type="checkbox"/>
DTIC TAB	<input type="checkbox"/>
Unannounced	<input type="checkbox"/>
Justification	
By .....	
Distribution/	
Availability Codes	
Dist	Avail and/or Special
A-1	

DTIC QUALITY INSPECTED 3

**TABLE OF CONTENTS**

**I. INTRODUCTION.....1**

**II. DEVELOPMENT.....3**

A. DEFINITIONS OF THE SYMBOLS.....3

B. IMAGE THEORY.....6

C. ACOUSTIC DOUBLET RADIATION WITHOUT  
REFLECTION COEFFICIENTS.....14

D. ACOUSTIC DOUBLET RADIATION ENCOUNTERING  
REFLECTION COEFFICIENTS.....17

E. DOWNSLOPE/UPSLOPE DOUBLET ANALYSIS OF  
THE IMAGE THEORY.....22

1. General Description.....22

2. Neutral Doublet Acoustic Field.....24

3. Acoustic Field from the Pairs of  
Acoustic Doublets Ignoring the  
Bottom Reflection Coefficients.....25

4. Acoustic Field from the Pairs of  
Acoustic Doublets Encountering the  
Bottom Reflection Coefficients.....29

**III. COMPUTER PROGRAMS.....30**

A. PROGRAM URTEXT.....30

B. PROGRAM URTEXT1.....32

C. PROGRAM URTEXT1C.....32

D. PROGRAM DOUBLT1C.....	32
E. PROGRAM CALL.....	34
F. PROGRAM PLOTIFD.....	34
<b>IV. VERIFICATION OF THE PROBLEMS.....</b>	<b>35</b>
A. COMPARISON BETWEEN THE IMAGE THEORY AND JAEGER'S PE MODEL WITH RESPECT TO THE ACOUSTIC DOUBLET RADIATION.....	35
1. Cases Tested.....	35
2. Specific Observations.....	35
B. CONTRIBUTION OF THE IMAGES.....	36
C. COMPARISON BETWEEN THE IMAGE THEORY AND THE DOUBLET ANALYSIS.....	37
<b>V. CONCLUSIONS AND RECOMMENDATIONS.....</b>	<b>51</b>
<b>APPENDIX A Tables.....</b>	<b>53</b>
<b>APPENDIX B Program URTEXT.....</b>	<b>58</b>
<b>APPENDIX C Program DOUBLT1C.....</b>	<b>67</b>
<b>LIST OF REFERENCES.....</b>	<b>76</b>
<b>INITIAL DISTRIBUTION LIST.....</b>	<b>77</b>

## LIST OF TABLES

### NUMERICAL RESULTS OF COMPARISON BETWEEN THE IMAGE THEORY AND THE DOUBLET ANALYSIS

1. Data for  $\beta=7^\circ$ ,  $\gamma=4^\circ$ ,  $R_1=4$ ,  $R_2=25$ ,  $\rho_1/\rho_2=0.7$ ,  
 $c_1=1500\text{m/s}$ ,  $c_2=1430\text{m/s}$ .....53
2. Data for  $\beta=6^\circ$ ,  $\gamma=2^\circ$ ,  $R_1=0.8$ ,  $R_2=5$ ,  $\rho_1/\rho_2=0.8$ ,  
 $c_1=1500\text{m/s}$ ,  $c_2=1450\text{m/s}$ .....54
3. Data for  $\beta=5^\circ$ ,  $\gamma=4^\circ$ ,  $R_1=2$ ,  $R_2=400$ ,  $\rho_1/\rho_2=0.6$ ,  
 $c_1=1500\text{m/s}$ ,  $c_2=1410\text{m/s}$ .....55
4. Data for  $\beta=4^\circ$ ,  $\gamma=1^\circ$ ,  $R_1=5$ ,  $R_2=12$ ,  $\rho_1/\rho_2=0.7$ ,  
 $c_1=1500\text{m/s}$ ,  $c_2=1420\text{m/s}$ .....56
5. Data for  $\beta=3^\circ$ ,  $\gamma=1^\circ$ ,  $R_1=1$ ,  $R_2=10$ ,  $\rho_1/\rho_2=0.9$ ,  
 $c_1=1500\text{m/s}$ ,  $c_2=1475\text{m/s}$ .....57

## LIST OF FIGURES

1.	Image Structure for a Wedge-shaped Duct.....	9
2.	Illustration of the Angles $\Theta_n$ , $\gamma$ , $\delta$ , and the Angle between the $n^{\text{th}}$ Image Plane and the Receiver.....	10
3.	The Angle of Incidence $\Theta_{\text{unn}}$ of the $n^{\text{th}}$ Upper Image on the $m^{\text{th}}$ Plane.....	11
4.	The Distance $R_{\text{un}}$ between Receiver and $n^{\text{th}}$ Upper Image.....	12
5.	Geometry Used in Deriving the Radiation Characteristics of an Acoustic Doublet, according to Eq.23.....	16
6.	Geometry Used in Deriving the Radiation Characteristics of an Acoustic Doublet, according to Eq.24.....	18
7.	Geometry Used in Deriving the Radiation Characteristics of an Acoustic Doublet, Including Reflection Coefficients, according to Eqs. 25 and 26.....	19
8.	Geometry Used in Deriving the Radiation Characteristics of an Acoustic Doublet, Including Reflection Coefficients, according to Eq.29.....	21



9.	Geometry Used in Deriving the Doublet Analysis.....	23
10.	Positions of the Receiver Considered in Program URTEXT.....	31
11.	Positions of the Receiver Considered in Program URTEXT1.....	33
12.	Downslope Transmission Loss (dB) vs Horizontal Source-Receiver Distance, to 200m, for $\beta=10^\circ$ , $\gamma=5.0384^\circ$ , $\rho_1/\rho_2=0.9$ , $C_1/C_2=0.9$ .....	40
13.	Downslope Transmission Loss (dB) vs Horizontal Source-Receiver Distance, to 1km, for $\beta=10^\circ$ , $\gamma=5.0384^\circ$ , $\rho_1/\rho_2=0.9$ , $C_1/C_2=0.9$ .....	41
14.	Downslope Transmission Loss (dB) vs Horizontal Source-Receiver Distance, to 10km, for $\beta=10^\circ$ , $\gamma=5.0384^\circ$ , $\rho_1/\rho_2=0.9$ , $C_1/C_2=0.9$ .....	42
15.	Downslope Transmission Loss (dB) vs Horizontal Source-Receiver Distance, to 1km, for $\beta=5^\circ$ , $\gamma=2.5048^\circ$ , $\rho_1/\rho_2=0.9$ , $C_1/C_2=0.9$ .....	43
16.	Downslope Transmission Loss (dB) vs Horizontal Source-Receiver Distance, to 10km, for $\beta=5^\circ$ , $\gamma=2.4952^\circ$ , $\rho_1/\rho_2=0.9$ , $C_1/C_2=0.9$ .....	44

17.	Downslope Transmission Loss	
	(dB) vs Horizontal Source-Receiver	
	Distance, to 1km, for $\beta=10^\circ$ , $\gamma=5.0384^\circ$ ,	
	$\rho_1/\rho_2=0.94$ , $C_1/C_2=0.94$ .....	45
18.	Downslope Transmission Loss	
	(dB) vs Horizontal Source-Receiver	
	Distance, to 10km, for $\beta=10^\circ$ , $\gamma=5.0384^\circ$ ,	
	$\rho_1/\rho_2=0.94$ , $C_1/C_2=0.94$ .....	46
19.	Downslope Transmission Loss	
	(dB) vs Horizontal Source-Receiver	
	Distance, to 1km, for $\beta=5^\circ$ , $\gamma=2.5048^\circ$ ,	
	$\rho_1/\rho_2=0.94$ , $C_1/C_2=0.94$ .....	47
20.	Downslope Transmission Loss	
	(dB) vs Horizontal Source-Receiver	
	Distance, to 10km, for $\beta=5^\circ$ , $\gamma=2.5048^\circ$ ,	
	$\rho_1/\rho_2=0.94$ , $C_1/C_2=0.94$ .....	48
21.	Downslope Transmission Loss	
	(dB) vs Horizontal Source-Receiver	
	Distance, to 10km, for $\beta=10^\circ$ , $\gamma=5.0384^\circ$ ,	
	$\rho_1/\rho_2=0.9999$ , $C_1/C_2=0.9999$ .....	49
22.	Downslope Transmission Loss	
	(dB) vs Horizontal Source-Receiver	
	Distance, to 10km, for $\beta=5^\circ$ , $\gamma=2.4952^\circ$ ,	
	$\rho_1/\rho_2=0.9999$ , $C_1/C_2=0.9999$ .....	50

## ACKNOWLEDGMENTS

I would like to thank Dr.A.B.Coppens for the direction and guidance he gave me to work on some new ideas during this research, and Dr.J.V.Sanders for his help in co-advising. I would like also to acknowledge the support of the Computer Center Department and especially that of Mrs. Helen M. Davis and Mr. Larry Frazier. Finally, I thank my wife Evi for her help in preparing the write-up of this thesis.

## I. INTRODUCTION

The propagation of sound in a wedge-shaped ocean is a very interesting problem, which is still being investigated. A better understanding will be significant for scientific research and military applications.

Both the image and parabolic equation (PE) models have been applied to this problem. Scientists who have been working with PE models are listed in refs. 1 and 2, and those with the image theory in refs. 3 through 7. At the Naval Postgraduate School (NPS), recent theses on this problem, are:

1. A PE model computer program developed by Larry Ernest Jaeger [Ref.2].
2. Three other theses mostly about the image theory, which are listed in refs. 5 through 7.

The most recent thesis was done by Kim Jong Rok, who, after a detailed development of the image theory, did a comparison between Jaeger's model and image theory, producing results for a frequency of 5Hz, a wedge angle of  $10^\circ$ , a source depth of 50m and various receiver depths. All analyses have shown that the image theory is acceptable.

This research will try to further verify the reliability of the image theory in various cases, to identify its behavior, and to develop an improved analysis based on this

theory. More specifically this thesis will address the following tasks:

1. Develop an image theory core program, which will be the basis of any future study. The associated computer program will be under the name UREXT.
2. Use acoustic doublet radiation to compare and analyze image theory results. This comparison assumes some matching of the water and fast bottom densities and sound velocities.
3. Verify the behavior of the sound field at points where total internal reflections from the first images start to contribute.
4. Extend a new analysis which combines the images in pairs of acoustic doublets, and compare with the original image theory.

## II. DEVELOPMENT

### A. DEFINITIONS OF THE SYMBOLS

The following symbols are used, (see Figs. 1 through 9), and all distances are scaled in terms of the scaling distance:

$\beta$	=	wedge angle	(Eq.1)
$R_1$	=	distance from apex to source	(Eq.9)
$R_2$	=	distance from apex to the receiver	(Eq.9)
$Y_0$	=	distance along the shore between the receiver and the source	(Eq.9)
$\gamma$	=	source angle measured downward from the surface	(Eq.7)
$\delta$	=	receiver angle measured downward from the surface	(Eq.9)
$\rho_1$	=	water density	(Eq.13)
$\rho_2$	=	bottom density	(Eq.13)
$c_1$	=	water sound speed	(Eq.13)
$c_2$	=	bottom sound speed	(Eq.13)
$\theta_c$	=	critical angle for fast bottom	(Eq.1)
$\theta_s$	=	"critical angle" for slow bottom (defined for convenience)	(Eq.4)
$\Theta_t$	=	transmission angle	(Eq.13)
$X_c$	=	scaling distance for fast bottom	(Eq.1)
$X_s$	=	scaling distance for slow bottom	

- (defined for convenience) (Eq.4)
- $k_1$  = wavenumber in the wedge (water) (Eq.1)
- $k_2$  = wavenumber in the bottom (Eq.2)
- $\alpha/k_2$  = loss term in the bottom (Eq.17)
- $n$  = image number in the description of the image theory, and pair of acoustic doublets number in the description of the doublet analysis (Eq.7,33)
- $\Theta_n$  = angle of the  $n^{\text{th}}$  image measured from the bottom (Eq.7)
- $R_{un}$  = distance between the receiver and the  $n^{\text{th}}$  upper image (Eq.9)
- $R_{ln}$  = distance between the receiver and the  $n^{\text{th}}$  lower image (Eq.10)
- $\Theta_{nm}$  = grazing angle of incidence on the  $m^{\text{th}}$  plane for the  $n^{\text{th}}$  image (Eq.13)
- $\Theta_{unm}$  = grazing angle of incidence on the  $m^{\text{th}}$  plane for the  $n^{\text{th}}$  upper image (Eq.11)
- $\Theta_{lnm}$  = grazing angle of incidence on the  $m^{\text{th}}$  plane for the  $n^{\text{th}}$  lower image (Eq.12)
- $R(\Theta_{unm})$  = reflection coefficient corresponding to  $\Theta_{unm}$  (Eq.18)
- $R(\Theta_{lnm})$  = reflection coefficient corresponding to  $\Theta_{lnm}$  (Eq.19)
- $P_u$  = complex pressure from the upper family of images (Eq.18)

$P_1$	=	complex pressure from the lower family of images	(Eq.19)
$d$	=	distance between the images of a doublet	(Eq.23)
$r_0$	=	distance of the neutral doublet (the source and its first surface reflected image) from the receiver	(Eq.31)
$\sigma_0$	=	receiver-neutral doublet axis angle	(Eq.31)
$\Gamma_0$	=	defined in page 24	
$r_n^+$	=	distance between the receiver and the $n^{\text{th}}$ upper doublet	(Eq.33)
$r_n^-$	=	distance between the receiver and the $n^{\text{th}}$ lower doublet	(Eq.34)
$r_{n0}$	=	distance between the receiver and the $n^{\text{th}}$ doublet, the receiver being on the surface ( $\delta=0$ ) for a given $R_2$	(Eq.35)
$\sigma_n^+$	=	receiver- $n^{\text{th}}$ upper doublet axis angle	(Eq.38)
$\sigma_n^-$	=	receiver- $n^{\text{th}}$ lower doublet axis angle	(Eq.39)
$\sigma_{n0}$	=	receiver- $n^{\text{th}}$ doublet axis angle, the receiver being on the surface ( $\delta=0$ ) for a given $R_2$ .	(Eq.40)
$\Gamma_n$	=	as defined in eq.45	
$\vartheta_n$	=	as defined in eq.46	
$\varphi_n$	=	as defined in eq.47	



$\epsilon_n$  = as defined in eq.48  
 $\xi_n$  = as defined in eq.49  
 $\chi, \psi$  = represent the different reflection coefficients of the images of an acoustic doublet (Eq.25)

$z$  = combined reflection coefficient for a doublet (Eq.26)

$\chi_n^+, \psi_n^+$  = reflection coefficients for the  $n^{\text{th}}$  upper doublet (Eq.52)

$\chi_n^-, \psi_n^-$  = reflection coefficients for the  $n^{\text{th}}$  lower doublet (Eq.52)

$P_n^+$  = complex pressure for the  $n^{\text{th}}$  upper doublet (Eq.43)

$P_n^-$  = complex pressure for the  $n^{\text{th}}$  lower doublet (Eq.44)

$P_n$  = complex pressure for the  $n^{\text{th}}$  pair of acoustic doublets (Eq.50)

It is worth noting that the source angle  $\gamma$  and the receiver angle  $\delta$  are measured downward from the surface, although in previous theses they were measured upward from the bottom. It was found more convenient to do so for the purposes of this research.

## B. IMAGE THEORY

The theoretical background of the image theory has been presented by Coppens, Sanders, Ioannou and Kawamura [Ref.3].

This section will be a brief review of the ideas and basic equations of the image theory.

The assumptions are:

1. The sound velocities and densities are constant both in the wedge and in the penetrable bottom.
2. The water-air boundary is a pressure release surface.
3. The slope is constant.
4. All boundaries are planar.

All distances are scaled, according to  $R_{scaled} = R_{real}/X$ . For a fast bottom, the scaling distance  $X_c$  is defined as the distance where the lowest mode attains cut off. For a slow bottom, the lowest mode does not attain cut off, but a scaling distance  $X_s$  is defined for convenience in calculations.

The definitions are

Fast bottom

$$k_1 X_c = \frac{\pi}{2 \sin \theta_c \tan \beta} \quad (1)$$

$$k_2 X_c = \frac{\pi}{2 \tan \theta_c \tan \beta} \quad (2)$$

$$\cos \theta_c = \frac{c_1}{c_2} \quad (3)$$

Slow bottom

$$k_1 X_s = \frac{\pi}{2 \tan \theta_s \tan \beta} \quad (4)$$

$$k_2 X_s = \frac{\pi}{2 \sin \theta_s \tan \beta} \quad (5)$$

$$\cos \theta_s = \frac{c_2}{c_1} \quad (6)$$

where  $\beta$  is the wedge angle, subscript 1 refers to the fluid in the wedge (water), and subscript 2 refers to the bottom.

The number of images, including the source, which contribute to the sound field, is given by  $n = \text{INT}(360^\circ/\beta)$ , (Fig.1). The angles between each image and the bottom (Figs. 1 through 3) are given by

$$\Theta_n = n\beta - \gamma, \quad \text{for } n \text{ odd} \quad (7)$$

$$\Theta_n = (n-1)\beta + \gamma, \quad \text{for } n \text{ even} \quad (8)$$

where  $\gamma$  is the angle of the source measured from the surface.

The distance between each image and the receiver (Figs. 2 and 4), is given by

$$R_{un} = \sqrt{R_1^2 + R_2^2 - 2R_1R_2 \cos(\Theta_n - \beta + \delta) + Y_0^2} \quad (9)$$

for the upper group of images, and

$$R_{ln} = \sqrt{R_1^2 + R_2^2 - 2R_1R_2 \cos(\Theta_n + \beta - \delta) + Y_0^2} \quad (10)$$

for the lower group of images, where  $R_1$  is the source-apex distance,  $R_2$  is the receiver-apex distance,  $\delta$  is the angle of the receiver from the surface, and  $Y_0$  is the horizontal

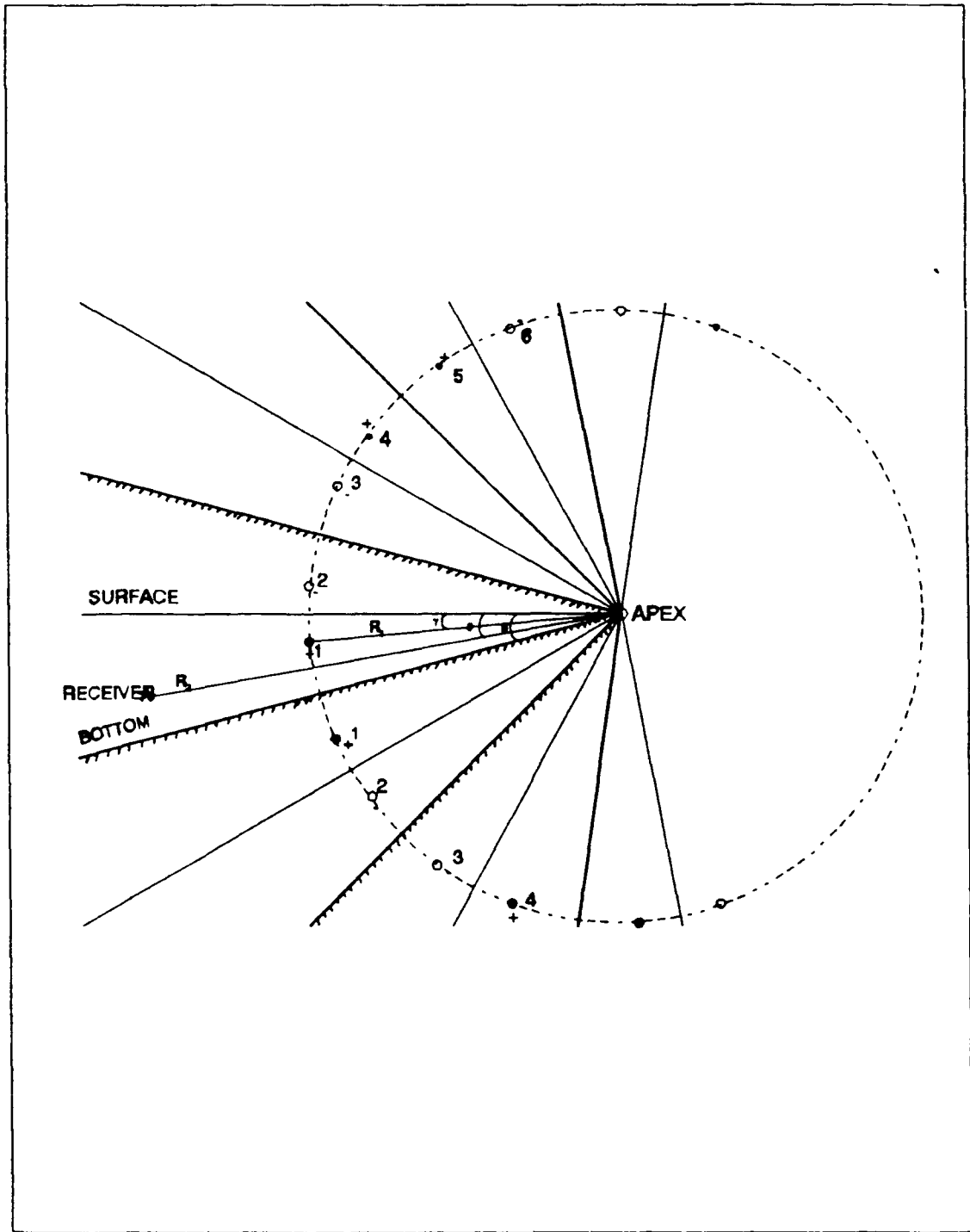
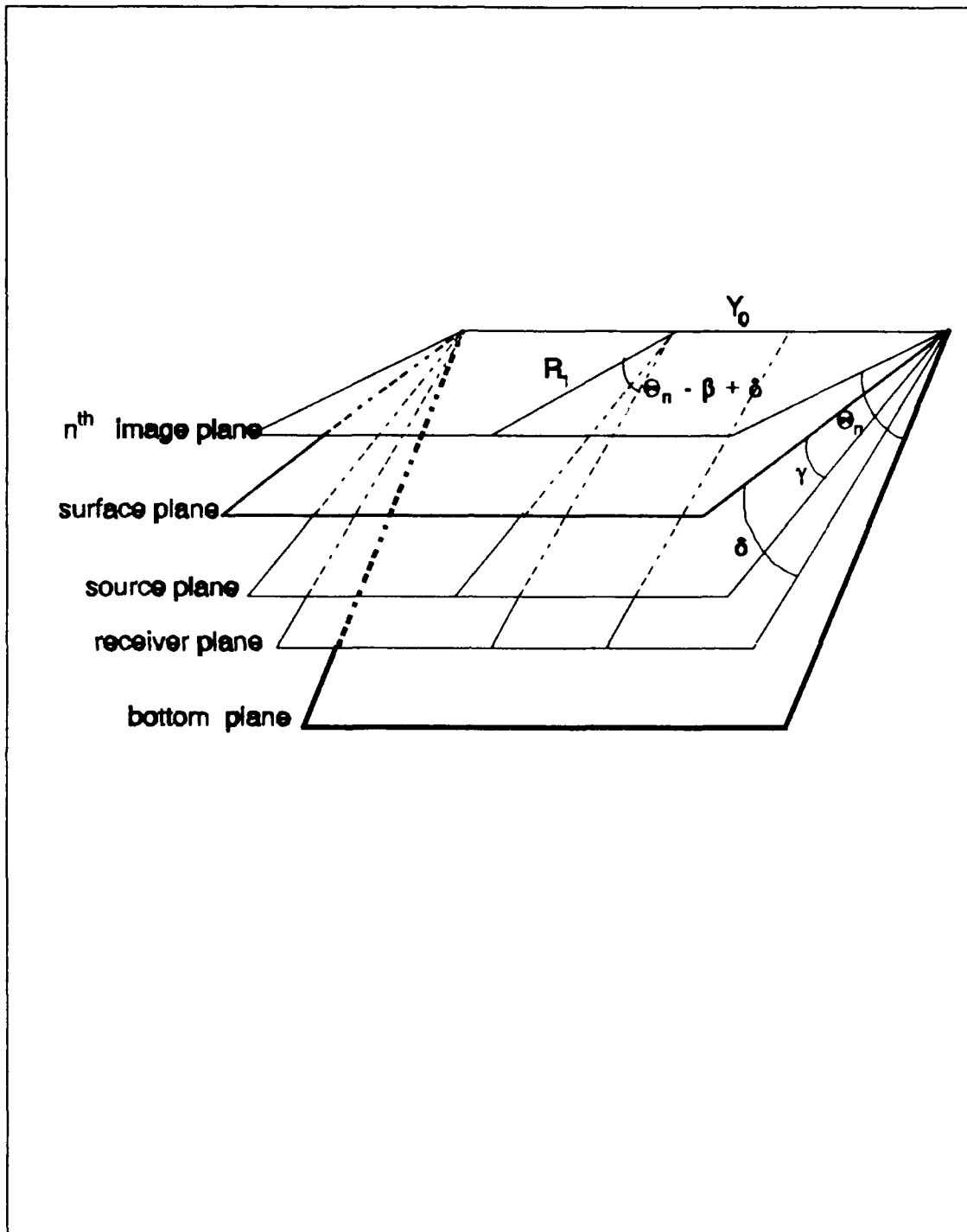


Figure 1. Image Structure for a Wedge-shaped Duct



**Figure 2.** Illustration of the Angles  $\theta_n$ ,  $\gamma$ ,  $\delta$ , and the Angle between the  $n^{\text{th}}$  Image Plane and the Receiver Plane.

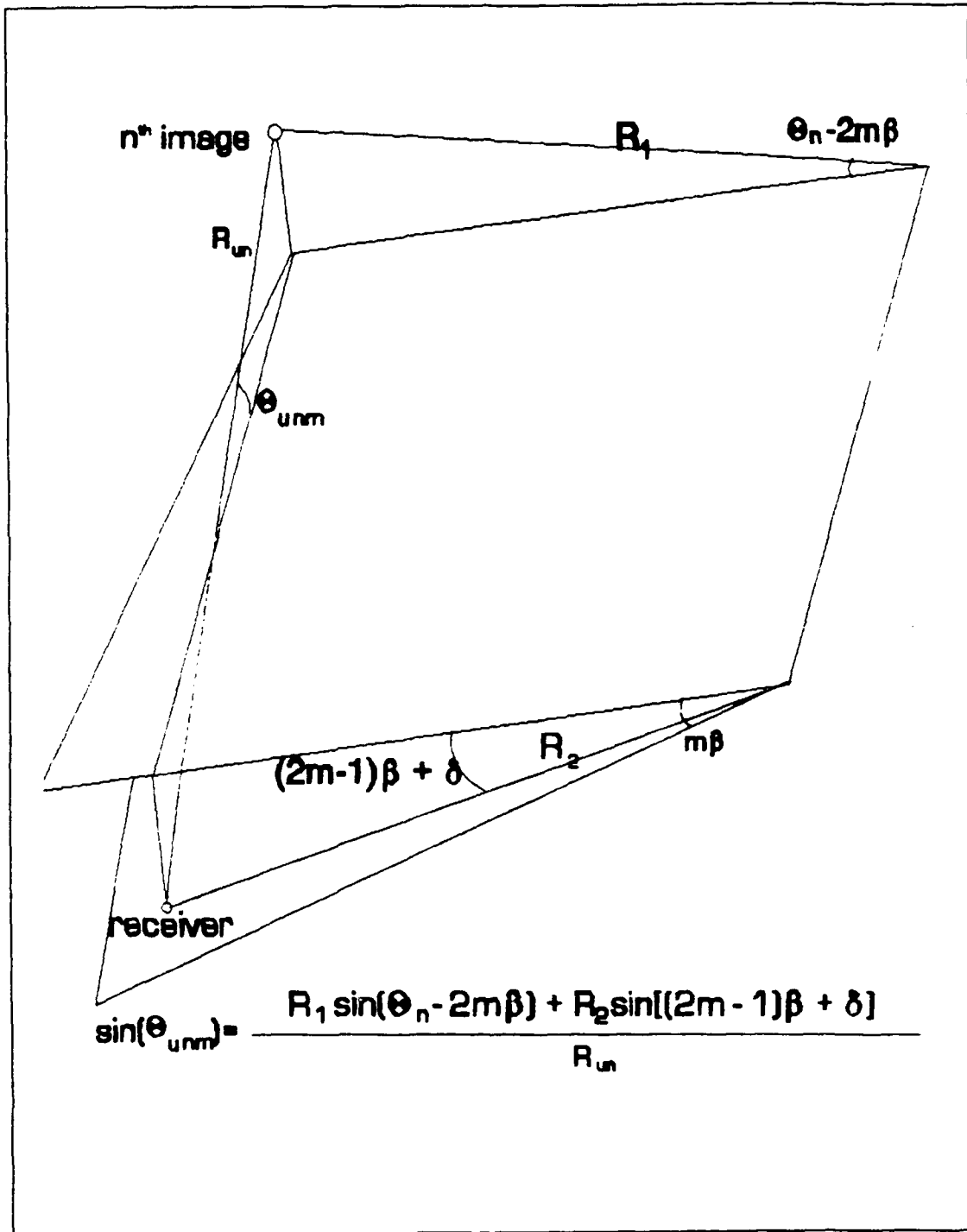
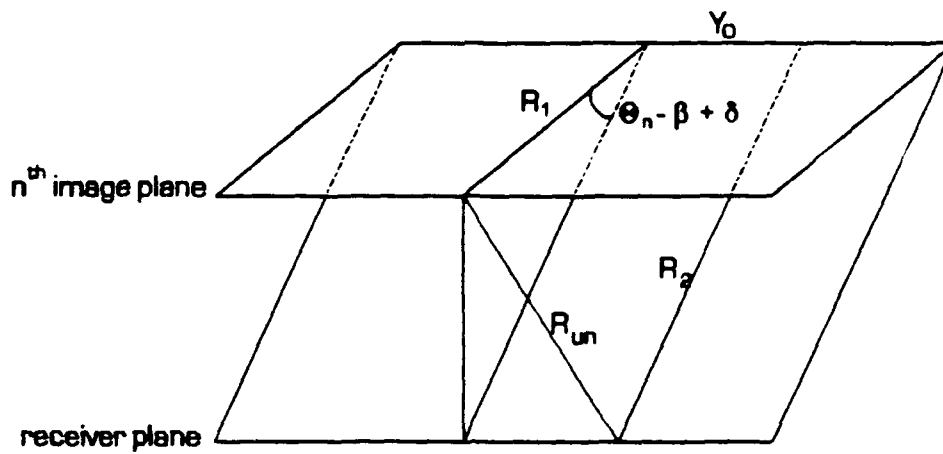


Figure 3. The Angle of Incidence  $\theta_{unm}$  of the  $n^{\text{th}}$  Upper Image on the  $m^{\text{th}}$  Plane.



$$R_{un} = \sqrt{R_1^2 + R_2^2 + Y_0^2 - 2 R_1 R_2 \cos(\theta_n - \beta + \delta)}$$

Figure 4. The Distance  $R_{un}$  between Receiver and  $n^{\text{th}}$  Upper Image.

source-receiver distance along the shore. All distances are scaled.

The incident angle of the  $n^{\text{th}}$  image to the  $m^{\text{th}}$  plane (Figs. 1 and 3), is given by

$$\sin(\Theta_{unm}) = \frac{R_1 \sin(\Theta_n - 2m\beta) + R_2 \sin[(2m-1)\beta + \delta]}{R_{un}}, \quad m=1, 2, \dots \quad (11)$$

for the upper group of images, and

$$\sin(\Theta_{lnm}) = \frac{R_1 \sin(\Theta_n - 2m\beta) + R_2 \sin[(2m+1)\beta - \delta]}{R_{ln}}, \quad m=0, 1, \dots \quad (12)$$

for the lower group of images.

The reflection coefficients are assumed to be the plane wave Rayleigh reflection coefficients, a good approximation for the problem. The equations for them are:

Without absorption

$$R(\Theta_{nm}) = \frac{\frac{\rho_2}{\rho_1} \sin(\Theta_{nm}) - \frac{c_1}{c_2} \sin(\Theta_t)}{\frac{\rho_2}{\rho_1} \sin(\Theta_{nm}) + \frac{c_1}{c_2} \sin(\Theta_t)} \quad (13)$$

$$\sin\Theta_t = \sqrt{1 - \left(\frac{c_2}{c_1}\right)^2 \cos^2(\Theta_{nm})} \quad (14)$$

where  $\Theta_{nm}$  is the incident grazing angle of the  $n^{\text{th}}$  image on the  $m^{\text{th}}$  plane (Fig.3) and  $\Theta_t$  is the corresponding transmission grazing angle.

With absorption



$$R(\Theta_{nm}) = \frac{\frac{\rho_2}{\rho_1} \sin \Theta_{nm} - \frac{1}{\sqrt{2}} \sqrt{\sqrt{b^2+a^2}+a} + j \frac{1}{\sqrt{2}} \sqrt{\sqrt{b^2+a^2}-a}}{\frac{\rho_2}{\rho_1} \sin \Theta_{nm} + \frac{1}{\sqrt{2}} \sqrt{\sqrt{b^2+a^2}+a} - j \frac{1}{\sqrt{2}} \sqrt{\sqrt{b^2+a^2}-a}} \quad (15)$$

$$a = (c_1/c_2)^2 - \cos^2 \Theta_{nm} \quad (16)$$

$$b = 2(c_1/c_2)^2 \alpha / k_2 \quad (17)$$

where  $\alpha$  is the absorption coefficient.

The total sound field pressure contribution from the upper images at each point in the wedge, is given by

$$P_u = \sum_{n=1}^N \frac{1}{R_{un}} \exp(-jk_1 R_{un}) (-1)^{(n/2)} \prod_{m=1}^M R(\Theta_{unm}) \quad (18)$$

$\prod R(\Theta_{unm}) = 1$ , for  $n = 1, 2$  and  $M = (n-1)/2$ ,

and from the lower images,

$$P_l = \sum_{n=1}^N \frac{1}{R_{ln}} \exp(-jk_1 R_{ln}) (-1)^{(n/2)} \prod_{m=0}^M R(\Theta_{lnm}) \quad (19)$$

The total pressure will be,  $P = P_u + P_l$ .

### C. ACOUSTIC DOUBLET RADIATION WITHOUT REFLECTION COEFFICIENTS

An acoustic doublet consists of two simple sources of equal strengths, separated by a distance  $d$ , vibrating with the same frequency but  $180^\circ$  out of phase with each other [Ref.8].

Assume as a reference that the source closer to the receiver is the negative one and the other one is the positive

(Fig.5). The pressure at point  $(r, \theta)$  due to the positive source is

$$P_1 = \frac{A}{r + \Delta r_1} e^{j(\omega t - k(r + \Delta r_1))} \quad (20)$$

and that due to the negative source is

$$P_2 = -\frac{A}{r - \Delta r_2} e^{j(\omega t - k(r - \Delta r_2))} \quad (21)$$

where  $r$  is the distance from the field point to the midpoint between the sources,  $\Delta r_1$  and  $\Delta r_2$  are as shown, and the opposite signs account for the phase difference of the sources. The acoustic doublet pressure at  $(r, \theta)$  is then

$$P = \frac{A}{r} \left( \frac{e^{-jk\Delta r_1}}{1 + \Delta r_1/r} - \frac{e^{jk\Delta r_2}}{1 - \Delta r_2/r} \right) e^{j(\omega t - kr)} \quad (22)$$

The process of replacing  $\Delta r_1$  and  $\Delta r_2$  by  $r$  and  $\theta$  is straightforward but tedious, and the resulting expression for  $p(r, \theta, t)$  is too complicated for efficient analysis. However, in the most frequently encountered cases, as it happens in the wedge-shaped ocean problem, the observation of the pressure is made at distances great compared to the separation of the sources. Therefore, it will be useful to derive the form of eq.22 suitable in the limit  $r \gg d$ . This is referred to as the far-field approximation. If  $r \gg d$ ,  $\Delta r_1 \approx \Delta r_2 \approx (d/2) \sin \theta$  and  $\Delta r_1/r \ll 1$ , so that eq.22 becomes

$$p(r, \theta, t) \approx -j \frac{2A}{r} \sin \left( \frac{1}{2} k d \sin \theta \right) e^{j(\omega t - kr)} \quad (23)$$

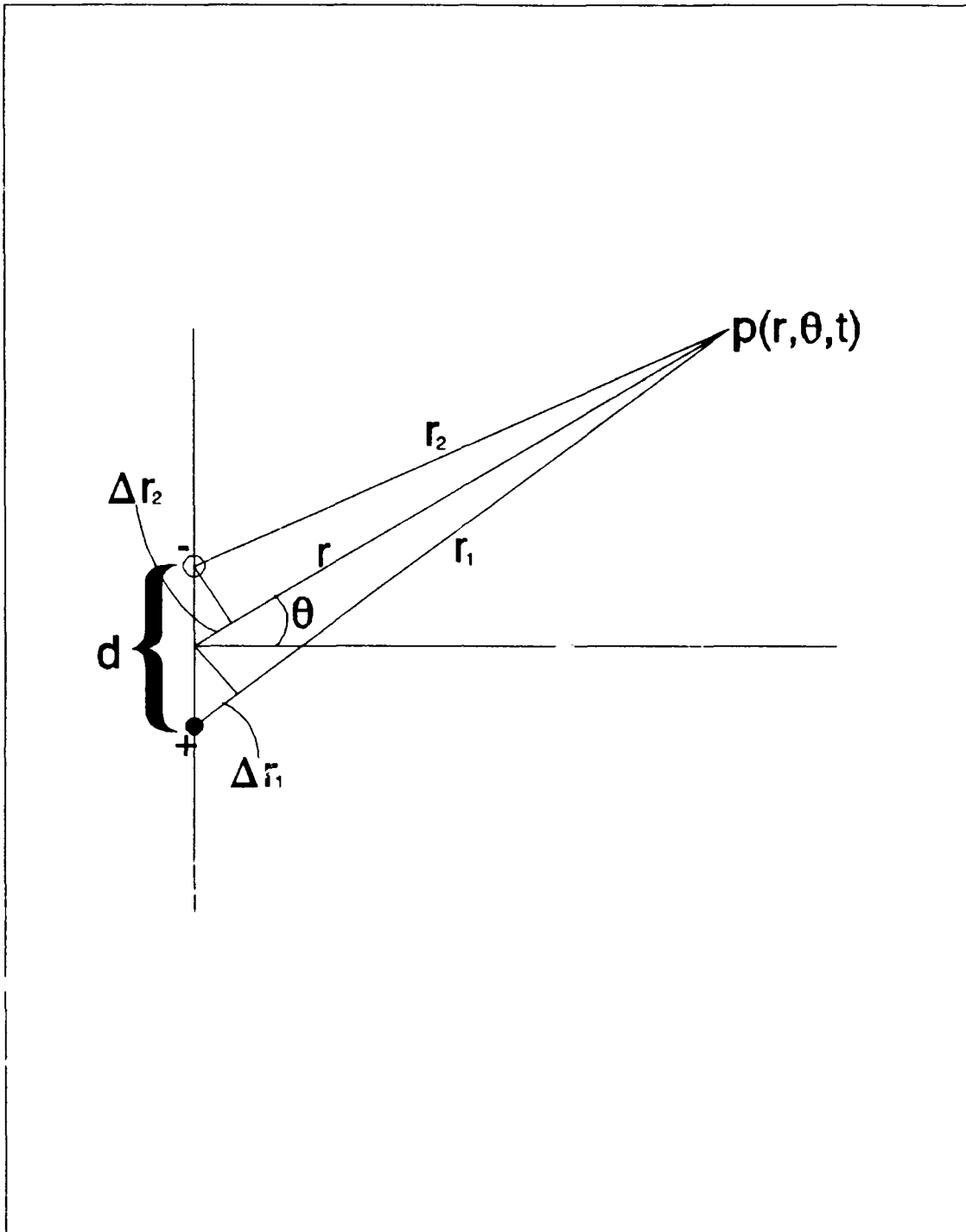


**Figure 5.** Geometry Used in Deriving the Radiation Characteristics of an Acoustic Doublet, according to Eq.23.

If the signs of the sources are reversed (Fig.6), then eq.23 changes sign too, and becomes

$$p(r, \theta, t) = j \frac{2A}{r} \sin\left(\frac{1}{2}kdsin\theta\right) e^{j(\omega t - kr)} \quad (24)$$

#### D. ACOUSTIC DOUBLET RADIATION ENCOUNTERING REFLECTION COEFFICIENTS

Consider again the situation of Fig.5, which was analyzed in the previous section. Suppose now that the free acoustic fields of the positive and negative sources encounter reflection coefficients  $\chi$  and  $\psi$  respectively. Those reflection coefficients are assigned to correspond to grazing angles  $\theta_\chi$ ,  $\theta_\psi$  as shown in Fig.7. Then eq.22 becomes

$$p = \frac{A}{r} \left( \chi \frac{e^{-jk\Delta r_1}}{1 + \Delta r_1/r} - \psi \frac{e^{jk\Delta r_2}}{1 - \Delta r_2/r} \right) e^{j(\omega t - kr)} \quad (25)$$

Combination of eq.23 and eq.25 gives

$$\frac{A}{r} \left( \chi \frac{e^{-j\frac{1}{2}kdsin\theta}}{1 + \Delta r_1/r} - \psi \frac{e^{j\frac{1}{2}kdsin\theta}}{1 - \Delta r_2/r} \right) = -j2 \frac{A}{r} z \sin\left(\frac{1}{2}kdsin\theta\right) \quad (26)$$

for the far field approximation ( $r \gg d$ ), where  $\Delta r_1 \approx \Delta r_2 \approx (1/2)dsin\theta$  and  $(\Delta r_1/r) \ll 1$ ,  $(\Delta r_2/r) \ll 1$ . The coefficient  $z$  is the appropriate reflection coefficient for the acoustic doublet field. After some mathematical manipulation of eq.26,

$$z = \frac{1}{2} [ (\chi + \psi) - j(\psi - \chi) \cot\left(\frac{1}{2}kdsin\theta\right) ] \quad (27)$$

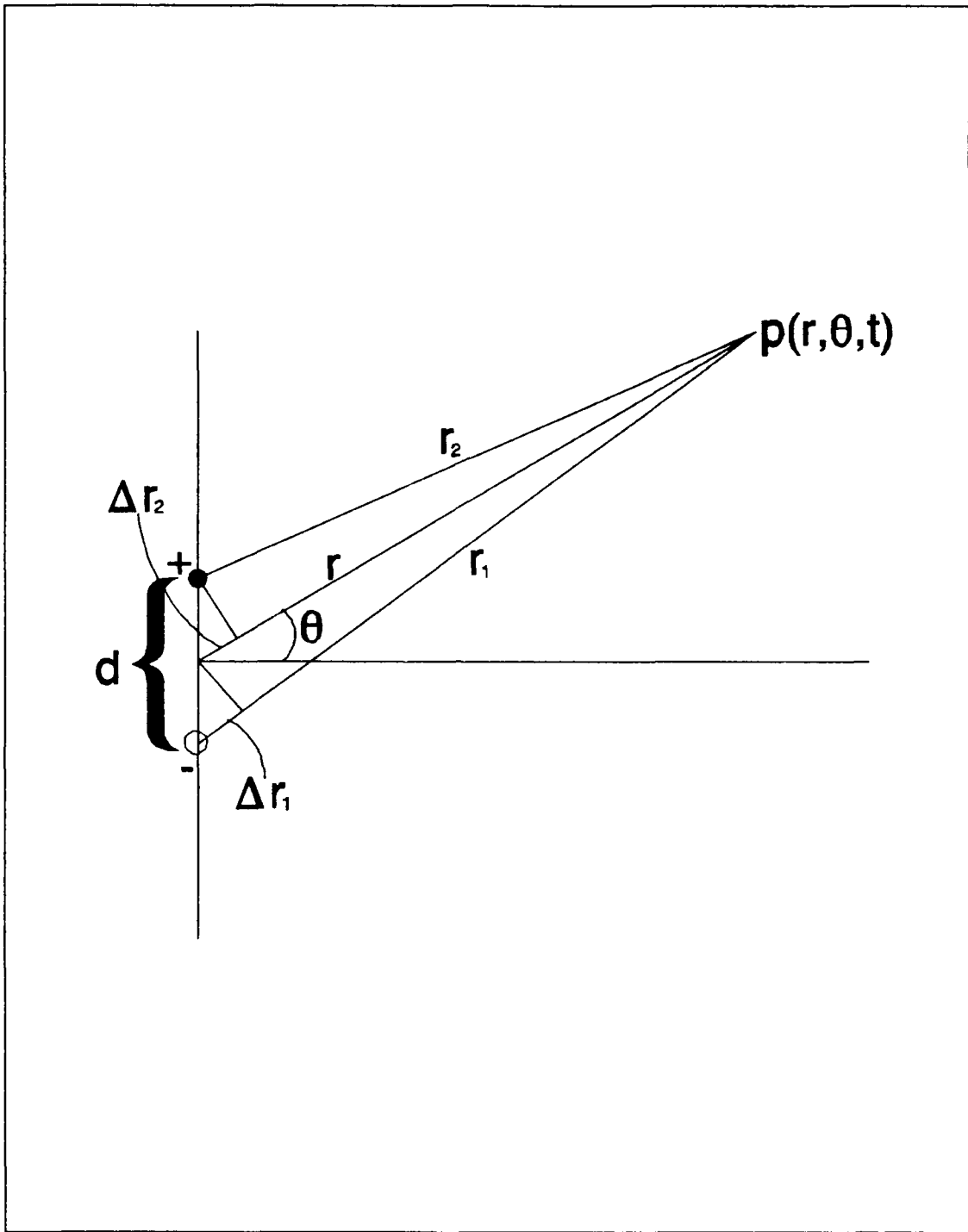


**Figure 6.** Geometry Used in Deriving the Radiation Characteristics of an Acoustic Doublet according to Eq.24.

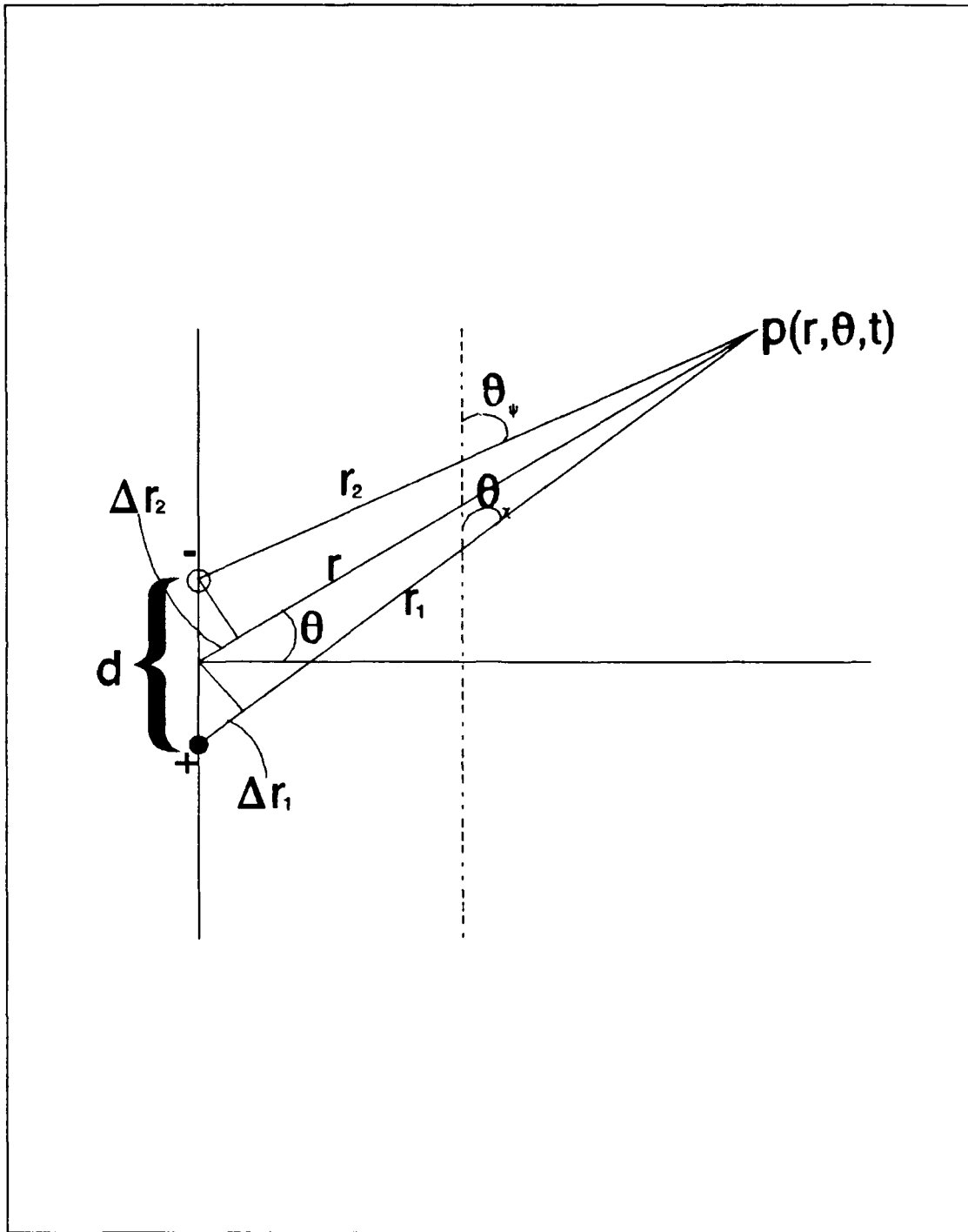


**Figure 7.** Geometry Used in Deriving the Radiation Characteristics of an Acoustic Doublet, Including Reflection Coefficients, according to Eqs. 25 and 26.

Suppose now that the polarity of the sources changes (Fig.8), and consider eq.24. In that case, the signs in both sides of eq.26 change, and the solution of eq.27 for the doublet reflection coefficient  $\underline{z}$  remains the same.

Surprisingly, this reflection coefficient didn't turn out to be too complicated to apply in the doublet analysis of the image theory, because it is expressed as a function of the sum and the difference of the reflection coefficients of the individual images in the doublet.

In this research, the choice for the difference was the reflection coefficient of the image closer to the receiver minus the reflection coefficient of the image further from the receiver. That can be seen from eq.27 in connection with Figs 7 and 8.

Combination of eq.27 with eqs. 23, 24 and 26, gives for the two different polarities the total acoustic doublet fields

$$p^- = -\frac{1}{r} [ (\psi - \chi) \cos\left(\frac{1}{2}kdsin\theta\right) + j(\chi + \psi) \sin\left(\frac{1}{2}kdsin\theta\right) ] e^{j(\omega t - kr)} \quad (28)$$

$$p^+ = \frac{1}{r} [ (\psi - \chi) \cos\left(\frac{1}{2}kdsin\theta\right) + j(\chi + \psi) \sin\left(\frac{1}{2}kdsin\theta\right) ] e^{j(\omega t - kr)} \quad (29)$$

with  $\underline{A}$  has been set equal to one.

These two equations were successfully applied in the doublet analysis of the image theory as will be discussed later.

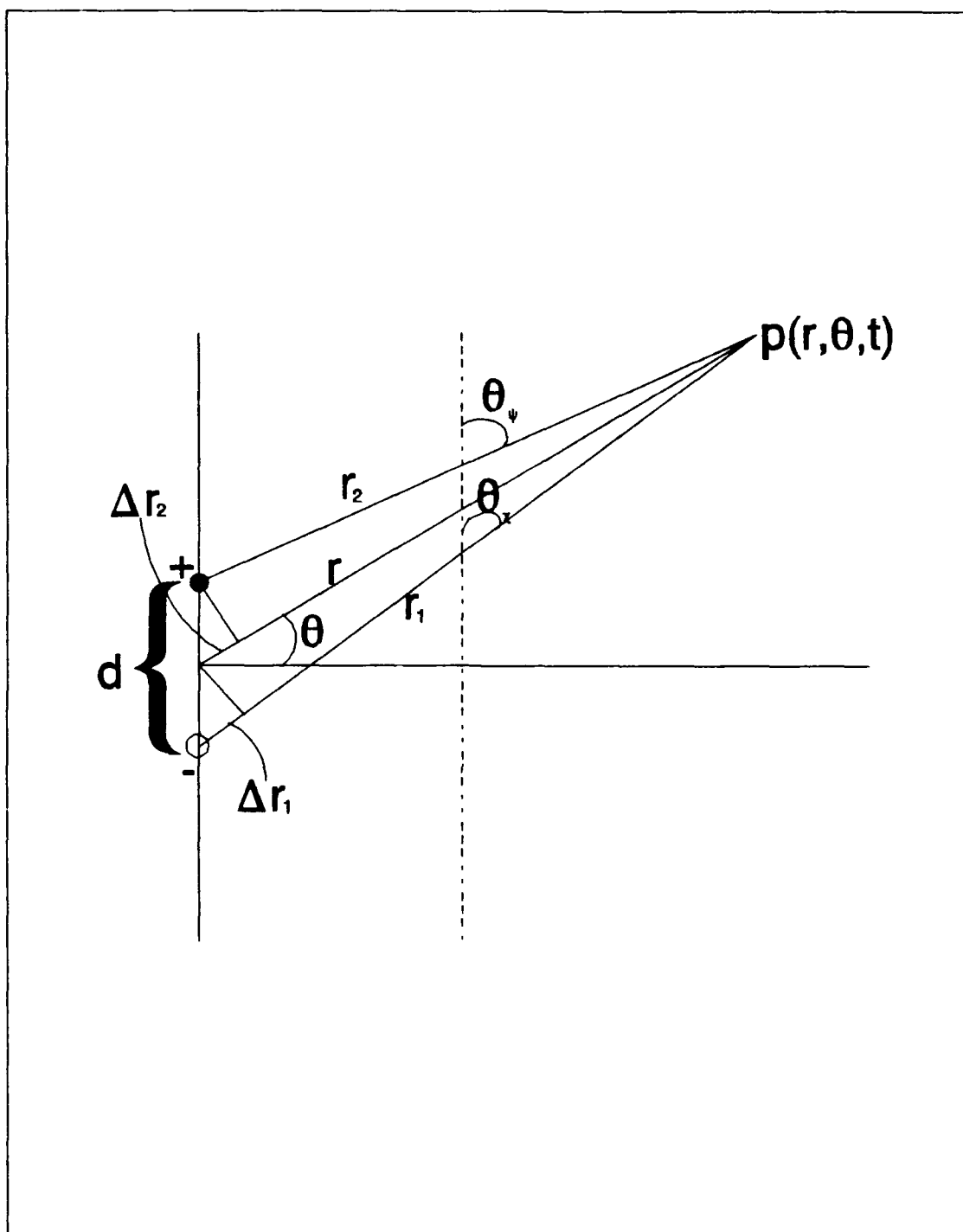


**Figure 8.** Geometry Used in Deriving the Radiation Characteristics of an Acoustic Doublet, Including Reflection Coefficients, according to Eq.29.



## E. DOWNSLOPE/UPSLOPE DOUBLET ANALYSIS OF THE IMAGE THEORY

### 1. General Description

The objective of this analysis is to combine the images in pairs of acoustic doublets and thus simplify the image theory [Ref.9].

The procedure starts (Fig.9) by first considering the 1<sup>st</sup> and 2<sup>nd</sup> upper images, the source and its first surface reflected image, as a neutral doublet. It is obvious that this neutral doublet (n=0) does not encounter any reflection coefficients.

The 3<sup>rd</sup> and 4<sup>th</sup> upper images (Fig.9) constitute the 1<sup>st</sup> upper doublet, and the 1<sup>st</sup> and 2<sup>nd</sup> lower images constitute the 1<sup>st</sup> lower doublet. Both doublets constitute the 1<sup>st</sup> pair of acoustic doublets (n=1). This procedure continues until all the images are organized in pairs of acoustic doublets.

The total number of pairs of acoustic doublets is

$$N = \text{Int} \left\{ \frac{[\text{Int} (\frac{360^\circ}{\beta}) - 2]}{4} \right\} \quad (30)$$

It is easily seen that in the worst case three images might be missed. In that case, those will be images at the end opposite to the source. Their contribution will be negligible, because many reflection coefficients will contribute to them, and among those reflection coefficients

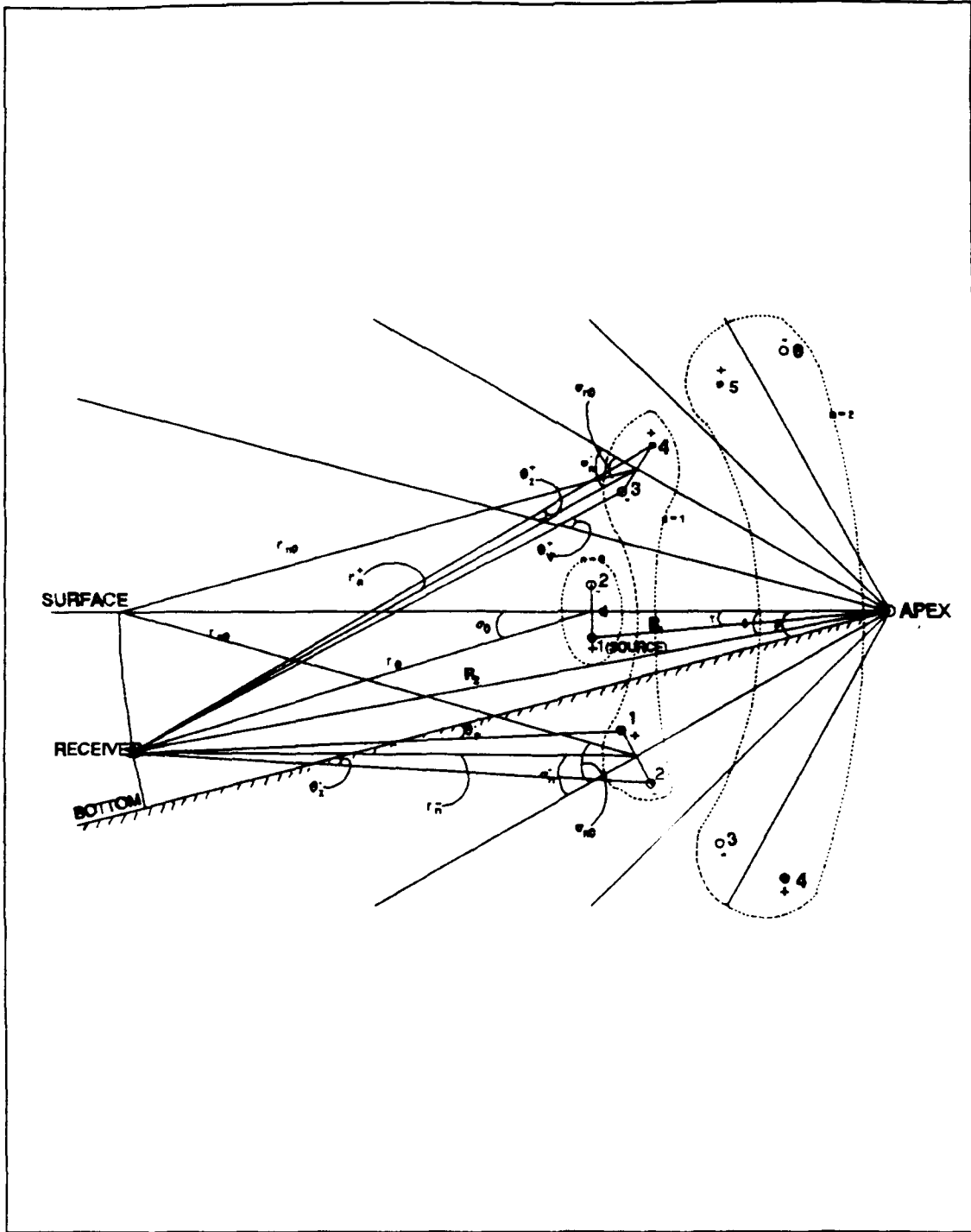


Figure 9. Geometry Used in Deriving the Doublet Analysis.

will be some with very small values. Hence, those images will be ignored.

## 2. Neutral Doublet Acoustic Field

The neutral doublet, which consists of the source and its first surface reflected image (Fig.9), does not encounter any reflection coefficients.

Application of eq.24 gives the pressure from the neutral doublet,

$$P_0 = +j \frac{2}{r_0} \sin \left( \frac{1}{2} k_1 d \sin \sigma_0 \right) e^{j(\omega t - k_1 r_0)} \quad (31)$$

$$\frac{d}{2} = R_1 \gamma, \quad \frac{1}{2} k_1 d = k_1 R_1 \gamma$$

$$\sin \sigma_0 = \frac{R_2}{r_0} \sin \delta = \frac{R_2}{r_0} \delta$$

$$\frac{1}{2} k_1 d \sin \sigma_0 = k_1 \frac{R_1 R_2}{r_0} \gamma \delta$$

If we define

$$\Gamma_0 = k_1 \frac{R_1 R_2}{r_0}$$

then the pressure has the simple form

$$P_0 = +j \frac{2}{r_0} \sin (\Gamma_0 \gamma \delta) e^{j(\omega t - k_1 r_0)} \quad (32)$$

where  $P_0$  is the neutral doublet complex pressure,  $r_0$  is its distance from the receiver, and  $\sigma_0$  is the receiver-doublet-

doublet axis angle. The positive sign in front of the right hand side of eq.31 and eq.32 counts for the positive reference of the source (Fig.9).

### 3. Acoustic Field from the Pairs of Acoustic Doublets Ignoring the Bottom Reflection Coefficients

The first pair of acoustic doublets is shown in Fig.9. The distances from the receiver of the individual upper and lower doublets at  $2n\beta$  are

$$r_n^+ = \sqrt{R_1^2 + R_2^2 - 2R_1R_2 \cos(2n\beta + \delta)} \quad (33)$$

for the upper doublet and

$$r_n^- = \sqrt{R_1^2 + R_2^2 - 2R_1R_2 \cos(2n\beta - \delta)} \quad (34)$$

for the lower doublet.

When the receiver is at the surface, then the above distances are equal

$$r_{n0} = \sqrt{R_1^2 + R_2^2 - 2R_1R_2 \cos(2n\beta)} \quad (35)$$

Eqs. 33 and 34 to the 2<sup>nd</sup> order approximation of the Taylor's series expansion around  $\delta=0$ , are

$$r_n = r_{n0} + \delta \left. \frac{dr_n}{d\delta} \right|_{\delta=0} + \frac{1}{2} \delta^2 \left. \frac{d^2 r_n}{d\delta^2} \right|_{\delta=0}$$

$$\left. \frac{dr_n^+}{d\delta} \right|_{\delta=0} = \frac{R_1 R_2}{r_{n0}} \sin(2n\beta)$$

$$\left. \frac{dr_n^-}{d\delta} \right|_{\delta=0} = -\frac{R_1 R_2}{r_{n0}} \sin(2n\beta)$$

$$\left. \frac{d^2 r_n^+}{d\delta^2} \right|_{\delta=0} = \left. \frac{d^2 r_n^-}{d\delta^2} \right|_{\delta=0} = \frac{R_1 R_2}{r_{n0}} [\cos(2n\beta) - \frac{R_1 R_2}{r_{n0}^2} \sin^2(2n\beta)]$$

$$r_n^+ = r_{n0} + \frac{R_1 R_2}{r_{n0}} \delta [\sin(2n\beta) + \frac{1}{2} \delta \cos(2n\beta) - \frac{1}{2} \delta \frac{R_1 R_2}{r_{n0}^2} \sin^2(2n\beta)] \quad (36)$$

$$r_n^- = r_{n0} + \frac{R_1 R_2}{r_{n0}} \delta [-\sin(2n\beta) + \frac{1}{2} \delta \cos(2n\beta) - \frac{1}{2} \delta \frac{R_1 R_2}{r_{n0}^2} \sin^2(2n\beta)] \quad (37)$$

Receiver-doublet-doublet axis angles are

$$\sin(\sigma_n^+) = \frac{R_2}{r_n^+} \sin(2n\beta + \delta) \quad (38)$$

for the upper doublet and

$$\sin(\sigma_n^-) = \frac{R_2}{r_n^-} \sin(2n\beta - \delta) \quad (39)$$

for the lower doublet.

When the receiver is at the surface this angle becomes the same for both doublets,

$$\sin(\sigma_{n0}) = \frac{R_2}{r_{n0}} \sin(2n\beta) \quad (40)$$

Eqs. 38 and 39 to the 1<sup>st</sup> order approximation of the Taylor's series expansion around  $\delta=0$  are

$$\sin(\sigma_n) \doteq \sin(\sigma_{n0}) + \delta \left. \frac{d\sin_n}{d\delta} \right|_{\delta=0}$$

$$\left. \frac{d\sin(\sigma_n^+)}{d\delta} \right|_{\delta=0} = \frac{R_2}{r_{n0}} \left[ \cos(2n\beta) - \frac{R_1 R_2}{r_{n0}^2} \sin^2(2n\beta) \right] \doteq \frac{R_2}{r_{n0}} \cos(2n\beta)$$

$$\left. \frac{d\sin(\sigma_n^-)}{d\delta} \right|_{\delta=0} = -\frac{R_2}{r_{n0}} \left[ \cos(2n\beta) - \frac{R_1 R_2}{r_{n0}^2} \sin^2(2n\beta) \right] \doteq -\frac{R_2}{r_{n0}} \cos(2n\beta)$$

$$\sin(\sigma_n^+) \doteq \frac{R_2}{r_{n0}} [\sin(2n\beta) + \delta \cos(2n\beta)] \quad (41)$$

$$\sin(\sigma_n^-) \doteq \frac{R_2}{r_{n0}} [\sin(2n\beta) - \delta \cos(2n\beta)] \quad (42)$$

The complex pressure field for the  $n^{\text{th}}$  upper doublet is

$$P_n^+ \doteq (-1)^n j \frac{2}{r_n^+} \sin \left[ \frac{1}{2} k_1 d \sin(\sigma_n^+) \right] e^{j(\omega t - k_1 r_n^+)} \quad (43)$$

and for the  $n^{\text{th}}$  lower doublet

$$P_n^- \doteq -(-1)^n j \frac{2}{r_n^-} \sin \left[ \frac{1}{2} k_1 d \sin(\sigma_n^-) \right] e^{j(\omega t - k_1 r_n^-)} \quad (44)$$

The approximation  $(1/2)k_1 d \doteq R_1 \gamma$  and the definition

$$\Gamma_n = k_1 \frac{R_1 R_2}{r_{n0}} \quad (45)$$

give

$$\vartheta_n = \Gamma_n \gamma \sin(2n\beta) \doteq \frac{1}{2} k_1 d \sin(\sigma_{n0}) \quad (46)$$

$$\varphi_n = \Gamma_n \delta \sin(2n\beta) \doteq k_1 \delta \left. \frac{dr_n}{d\delta} \right|_{\delta=0} \quad (47)$$

$$\varepsilon_n = \Gamma_n \gamma \delta \cos(2n\beta) \doteq \left( \frac{1}{2} k_1 d \right) \delta \left. \frac{d \sin \sigma_n}{d\delta} \right|_{\delta=0} \quad (48)$$

$$\xi_n = \frac{1}{2} \left( \frac{\delta \varepsilon_n}{\gamma} - \frac{\varphi_n^2}{k_1 r_{n0}} \right) \doteq \frac{1}{2} k_1 \delta^2 \left. \frac{d^2 r_n}{d\delta^2} \right|_{\delta=0} \quad (49)$$

The above approximations and the definitions in eqs. 45 through 49, give the pressure field for the  $n^{\text{th}}$  pair of acoustic doublets (the sum of the pressure fields of the corresponding upper and lower doublets)

$$P_n = P_n^+ + P_n^- \doteq (-1)^n j \frac{2}{r_{n0}} e^{j(\omega t - k_1 r_{n0} - \xi_n)} [e^{-j\varphi_n} \sin(\vartheta_n + \varepsilon_n) - e^{j\varphi_n} \sin(\vartheta_n - \varepsilon_n)] \quad (50)$$

More specifically, the following approximations were applied in eq. 50:

1.  $r_{n0}$  used in amplitude ( $2/r_{n0}$ ), instead of  $r_n^+$  and  $r_n^-$ .
2.  $r_n$  correct to the 2<sup>nd</sup> order approximation ( $\xi_n$ ) in phase.
3.  $\sigma_n$  correct to the 1<sup>st</sup> order approximation ( $\varepsilon_n$ ) in amplitude.

The total field is the sum over all pairs of acoustic doublets, plus the field of the neutral doublet:

$$P = P_0 + \sum_{n=0}^N [P_n^+ + P_n^-] \quad (51)$$

**4. Acoustic Field from the Pairs of Acoustic Doublets Encountering the Bottom Reflection Coefficients.**

The reflection coefficient of eq.27 is applied to eq.50. Hence, according to eqs. 28 and 29, the pressure field including the bottom reflection coefficients is

$$P_n = (-1)^n \frac{1}{r_{n0}} e^{j(\omega t - k_1 r_{n0} - \frac{1}{2}\pi)} \left\{ e^{-j\vartheta_n} [(\cos(\vartheta_n + \varepsilon_n)) (\psi_n^+ - \chi_n^+) + j(\sin(\vartheta_n + \varepsilon_n)) (\chi_n^+ + \psi_n^+)] - e^{j\vartheta_n} [(\cos(\vartheta_n - \varepsilon_n)) (\psi_n^- - \chi_n^-) + j(\sin(\vartheta_n - \varepsilon_n)) (\chi_n^- + \psi_n^-)] \right\} \quad (52)$$

where  $\psi_n^+$ ,  $\psi_n^-$  are the reflection coefficients of the upper and lower doublet images closer to the receiver, and  $\chi_n^+$ ,  $\chi_n^-$  are those further from the receiver. The corresponding grazing angles  $\theta_\chi^+$ ,  $\theta_\chi^-$ ,  $\theta_\psi^+$ ,  $\theta_\psi^-$  are illustrated in Fig.9.

The total field is given by eq.51, where  $P_n = P_n^+ + P_n^-$  is given by eq.52.



### III. COMPUTER PROGRAMS

The following computer programs, were created and used during this research. They were written in the FORTRAN 77 computer language, on the IBM-3033 main frame NPS computer system. Some of the programs use plotting routines, using the DISSPLA graphics package, while URTEXT and DOUBLT1C do not. Copies of all programs are available in professors Coppens main frame account.

#### A. PROGRAM URTEXT

In the beginning, the program URTEXT was created to provide a well documented, immutable program of the wedge-shaped ocean image theory. The follow-on programs are modifications of URTEXT.

In URTEXT, the receiver, at distance  $R_2$  from the apex, moves from the surface to the bottom of the wedge, on a circular arc (Fig.10). This program provides two distinct results of the image theory:

1. Pressure amplitude vs receiver angle.
2. Phase vs receiver angle.

The receiver angle is measured downward from the surface. This program accepts input data and also gives the output data

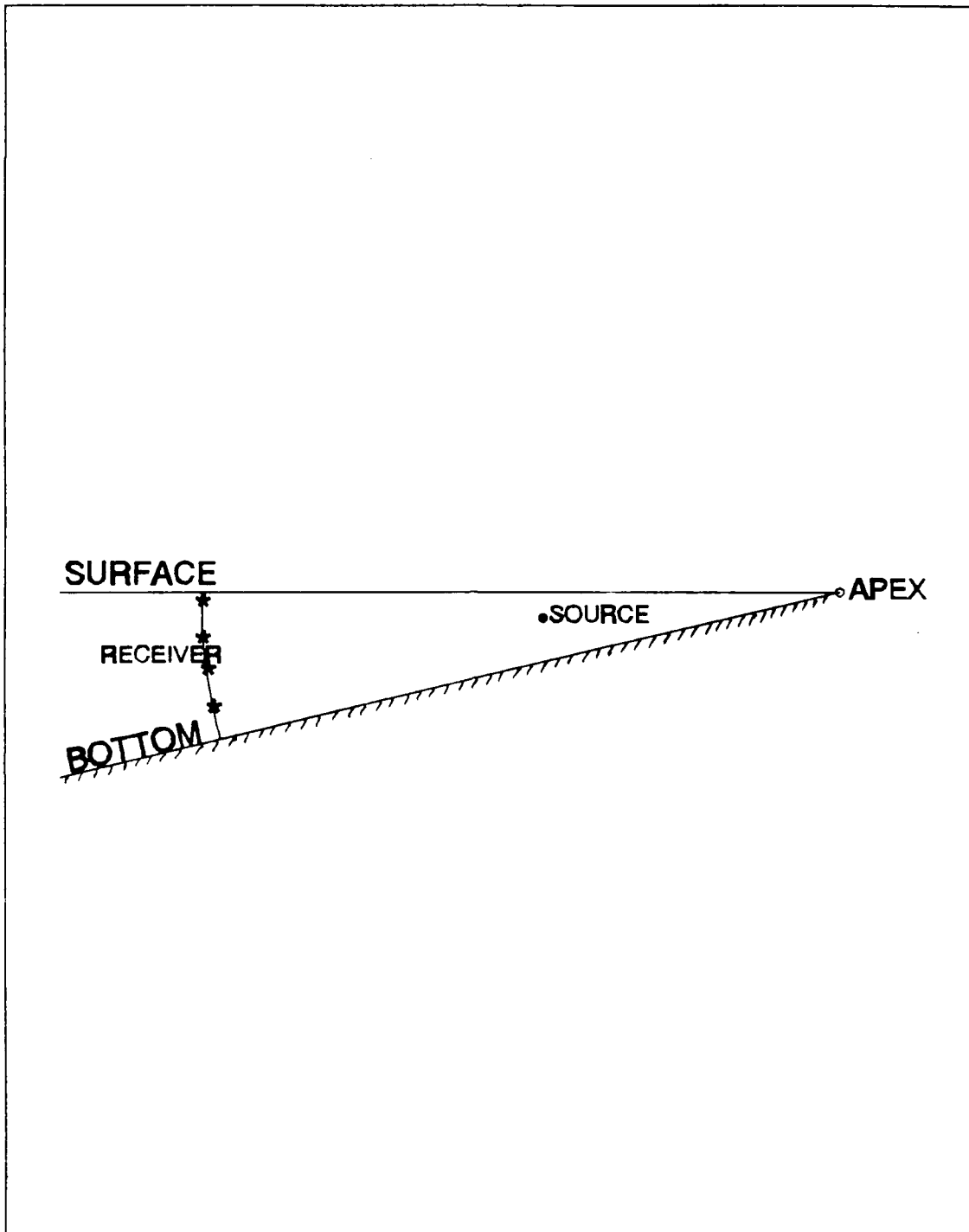


Figure 10. Positions of the Receiver Considered in Program URTEXT.

with respect to the scaling distance, independent of the frequency. Appendix "B" is a copy of URTEXT.

#### **B. PROGRAM URTEXT1**

In this program the receiver moves horizontally. Hence, its depth from the surface is kept constant (Fig.11). This program provides two distinct results for comparison:

1. Transmission loss (TL) vs source-receiver horizontal range, using the complete image theory.
2. Transmission loss (TL) vs source-receiver horizontal range, using only the neutral doublet acoustic radiation.

The inputs and outputs are frequency dependent and distances are expressed in meters or kilometers.

#### **C. PROGRAM URTEXT1C**

In this program, the receiver moves as does in URTEXT and it provides the same results. The only difference is the addition of a plotting routine, to present the data.

#### **D. PROGRAM DOUBLT1C**

In this program, the receiver moves the same as in URTEXT, and it also provides the same results. The calculations are done according to the doublet analysis presented previously, without including any absorption in the bottom ( $\alpha/k_2=0$ ) or in the water. The reflection coefficient used, was that of

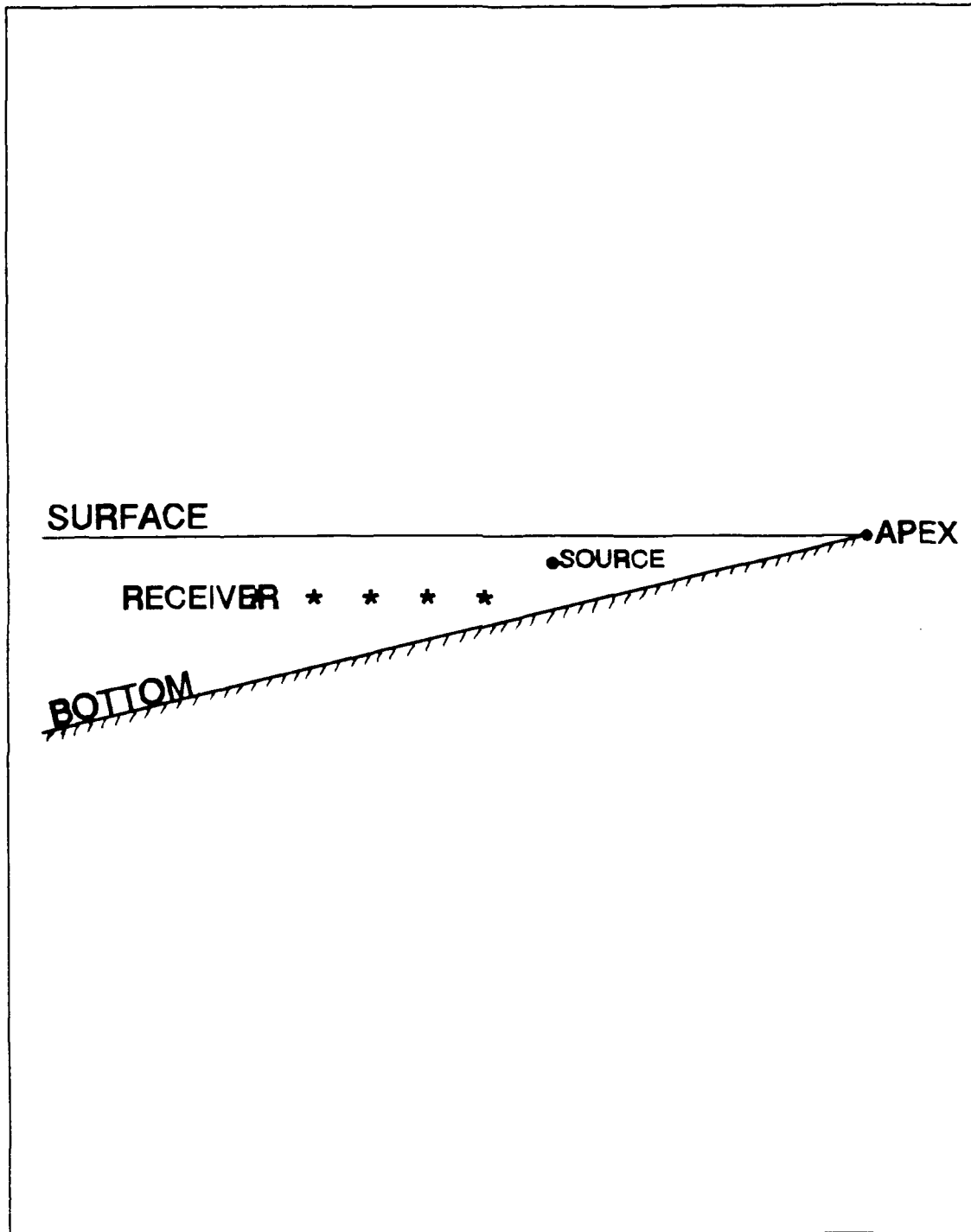


Figure 11. Positions of the Receiver Considered in Program URTEXT1.

equation 13. It works for a slow bottom only. It was used with their real reflection coefficients, this program was used to simplify the initial verification of the doublet analysis. Appendix "C" is a copy of this program.

#### **E. PROGRAM CAL1**

This program calculates the cosine of the incident grazing angle of the  $n^{\text{th}}$  image on the  $m^{\text{th}}$  plane, as a function of range. It was used to determine at what range from the source the total reflection contribution from the first images starts, as a function of the critical angle, defined as  $\cos\theta_c = c_1/c_2$ .

#### **F. PROGRAM PLOTIFD**

This is a plotting program developed by Jaeger to plot his PE model's data. It was modified to overplot URTEXT1 data for comparison.

#### IV. VERIFICATION OF THE PROBLEMS

##### A. COMPARISON BETWEEN THE IMAGE THEORY AND JAEGER'S PE MODEL WITH RESPECT TO THE ACOUSTIC DOUBLET RADIATION.

This was done by using the URTEXT1, JAEGER and PLOTIFD programs.

###### 1. Cases Tested

The cases tested (Figs. 12 to 22) were:

1. Wedge angles  $\beta = 10^\circ$  and  $\beta = 5^\circ$ .
2. Frequency  $f = 50$  Hz.
3. Source depth = 50 m.
4. Source angles  $\gamma = 2.4952^\circ, 2.5048^\circ, 5.0384^\circ$ .
5. Receiver depth = 75 m.
6.  $D1 = \rho_1/\rho_2 = 0.9, 0.94, 0.9999$ .
7.  $CC = c_1/c_2 = 0.9, 0.94, 0.9999$ .
8. Source-receiver horizontal ranges from 0-1 km and from 0-10 km, downslope.

In these figures, the dashed line represents the image theory data, the dotted line represents the doublet (source and first surface reflected image) data, and the solid line represents the Jaeger's PE model data.

###### 2. Specific Observations

1. In close distances from 0-200 m (Figs. 12 and 13), the image theory is almost in agreement with the acoustic

doublet radiation curve, while the PE model does not agree very well.

2. At larger distances, it is hard to say if the image theory or PE model is better, because the contribution of the images becomes significant. More specifically:
  - a. The two TL curves seem to agree with each other, being far away from that of the acoustic doublet.
  - b. In almost identical matching,  $D_1=0.9999$ ,  $CC=0.9999$  and at  $\beta=10^\circ$  (Fig.21), all three curves were perfectly coincident. The same case at  $\beta=5^\circ$  (Fig.22), gave a difference between the image theory and the acoustic doublet, starting from about 3 km, and reaching about 2.5 db at 10.0 km, but gave a good coincidence up to 3 km. This might have happened due to the more significant contribution of more images at larger distances.
3. For  $\beta=10^\circ$  and  $D_1=0.9$ ,  $CC=0.9$  or closer to unity, for short ranges up to 100 m, the effects of the bottom can be ignored with very small error.

#### B. CONTRIBUTION OF THE IMAGES

By using the program CAL1, some calculations were made of the grazing angle of the  $n^{\text{th}}$  image with the  $m^{\text{th}}$  plane versus range. When this angle is equal to the  $\theta_c$ , this is the range where total internal reflection of the image starts. This test was made for the 1<sup>st</sup> and 2<sup>nd</sup> lower images and the 3<sup>rd</sup> upper image, because these contribute most significantly. The following observations, were done for the cases considered previously:

1. At  $\beta=10^\circ$ ,  $CC=0.9$ , the 1<sup>st</sup> lower image contributes total reflection at 236 m, the 2<sup>nd</sup> lower image at 533 m, and the 3<sup>rd</sup> upper image at 764 m. Almost at those locations three characteristic bumps appear on the image theory TL curve for that case (Fig.13). On the PE model curve the first bump appears correctly, the second did not appear, and the third appears with a difference of 33 m (Fig.13).

2. The same case was tested at  $\beta=5^\circ$ ,  $CC=0.9$ , and the distances obtained were 187 m, 427 m, 581 m. The image theory TL curve's bumps correctly appeared almost at those distances (Fig.15).

All tests done above show that the image theory behaves as expected. Hence, it is reconfirmed that it is deemed worthy to be applied in the wedge-shaped ocean problem.

### C. COMPARISON BETWEEN THE IMAGE THEORY AND THE DOUBLET ANALYSIS

This comparison was done using the results of URTEXT1C and DOUBLT1C. Some of the results obtained can be seen in Tables 1 to 5, in Appendix "A". Those tables clearly show the excellent agreement between the two programs. Many other cases were tested to verify those results, but are not included in this thesis. All results that were tested were in agreement. More specifically:

1. In all cases tested, there was an excellent agreement in amplitude, as it can be seen from some data collected in Tables 1 to 5.
2. Although very good agreement (3<sup>rd</sup> decimal) is still valid in amplitude when the source gets close to the bottom, in that case appears a phase difference not larger than  $30^\circ$  in most cases tested. An example can be seen in the data collected in Table 1. The reduced accuracy of the doublet approximation (Eqs. 23 and 24), due to the larger  $d$ , is not responsible, because the phase difference does not disappear even when  $R_2 - R_1 \gg d$ . It was seen that with higher order approximations of the Taylor's series expansion of  $r_n$ ,  $\sigma_n$  in both phase and amplitude of eq.52, that phase difference reduces. Probably, it is not worth complicating the analysis by including these higher orders, because the accuracy as it exists will be acceptable in most practical cases. Also note that only



the amplitude is necessary for the calculation of the transmission loss, and that is obtained with excellent accuracy.

Because of the good agreement described previously, the doublet analysis can be used as a substitute of the full image theory.

During this research, efforts were made to simplify the doublet analysis. It was found that the approximations described in sect. E of the development, can not be simplified to give correct results everywhere in the wedge.

Consider the grazing angles formed between  $r_n^+$  and bottom planes for the upper doublets, and between  $r_n^-$  and bottom planes for the lower doublets (Fig.9). A further simplification of the doublet reflection coefficients could be accomplished by considering that the reflection coefficients correspond to these grazing angles. This method gives correct results only under the follow conditions:

1. Large wedge angles ( $\beta > 5^\circ$ ), which usually are not met in practice.
2. The receiver shallower than the surface-bottom middle depth.
3.  $R_1/R_2 \ll 1$  cannot hold for the downslope case, nor  $R_1/R_2 \gg 1$ , for the upslope case.

It was not possible to determine an exact threshold to apply such an approximation, because the total field is calculated encountering multiple factors. For that reason, the reflection coefficient as given in eq.27 was used. Some

explanations of the necessity to use eq.27 for the reflection coefficient, can be derived by examining eq.28. This equation is reproduced here without the phase factor  $e^{j(\omega t - kx)}$ :

$$p^- = -\frac{1}{r} [(\psi - \chi) \cos(\frac{1}{2}kdsin\theta) + j(\chi + \psi) \sin(\frac{1}{2}kdsin\theta)]$$

$\chi + \psi$  is always greater than  $\psi - \chi$ , for real reflection coefficients. The smaller the difference between the reflection coefficients  $\chi, \psi$  of the images in the doublet, the more dominant the imaginary part of the above equation will be, with respect to  $\chi, \psi$ .

Consider now, small wedge angles ( $\beta < 5^\circ$ ), along with  $R_1 \ll R_2$  for downslope and  $R_1 \gg R_2$  for upslope. Due to the small wedge angle, the lower images contribute significantly. Then, for these lower images,  $\cos[(1/2)kdsin\theta] \rightarrow 1$  and  $\sin[(1/2)kdsin\theta] \rightarrow 0$ , because of the small value of the receiver-doublet axis angle, under the above conditions. Therefore, in that case, the real part will be more dominant.

It becomes clear from the above discussion, that in many cases, neither the real or the imaginary parts of eq.28 can be ignored. Thus, eq.28 is the correct equation to apply for the wedge.

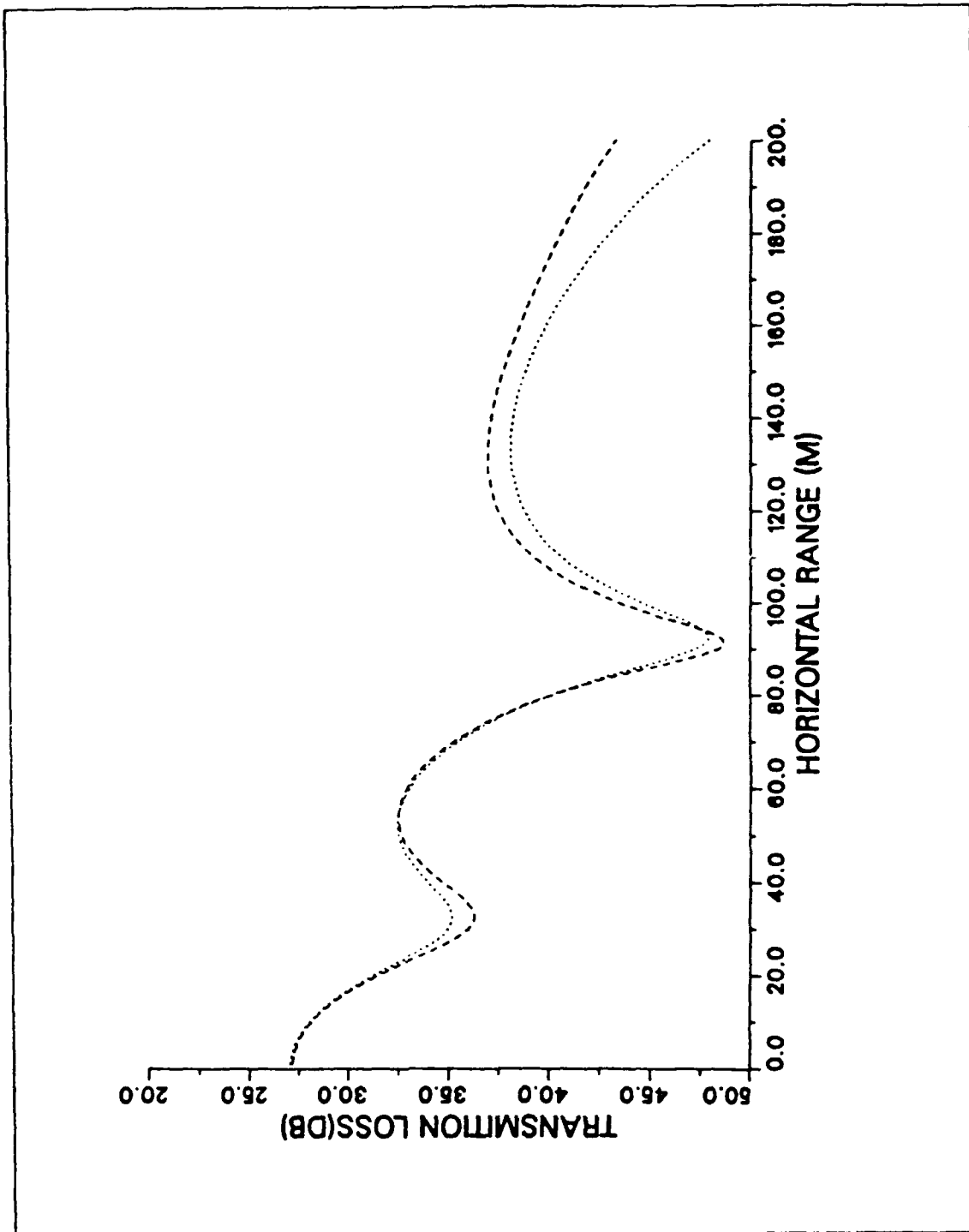


Figure 12. Downslope Transmission Loss (dB) vs Horizontal Source-Receiver Distance, to 200m, for  $\beta=10^\circ$ ,  $\gamma=5.0384^\circ$ ,  $\rho_1/\rho_2=0.9$ ,  $C_1/C_2=0.9$ .

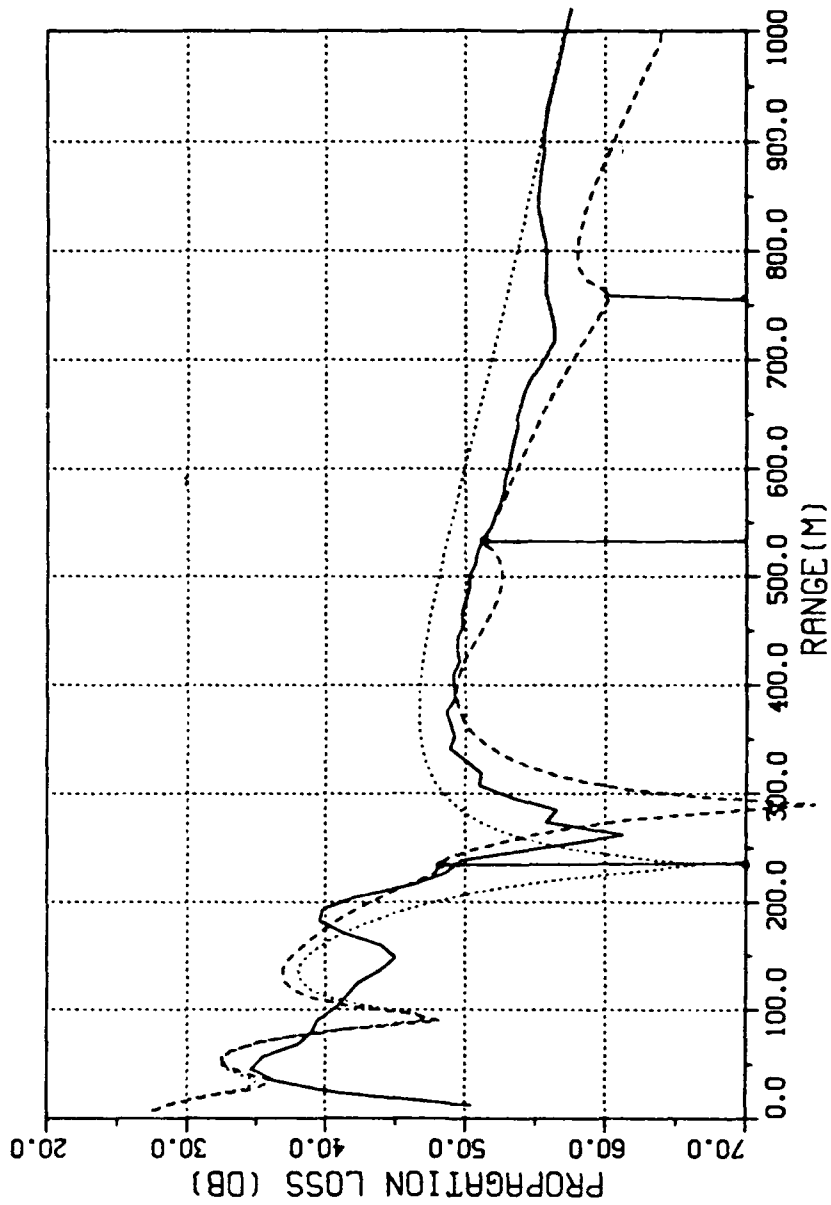


Figure 13. Downslope Transmission Loss (dB) vs Horizontal Source-Receiver Distance, to 1km, for  $\beta=10^\circ$ ,  $\gamma=5.0384^\circ$ ,  $\rho_1/\rho_2=0.9$ ,  $C_1/C_2=0.9$ .

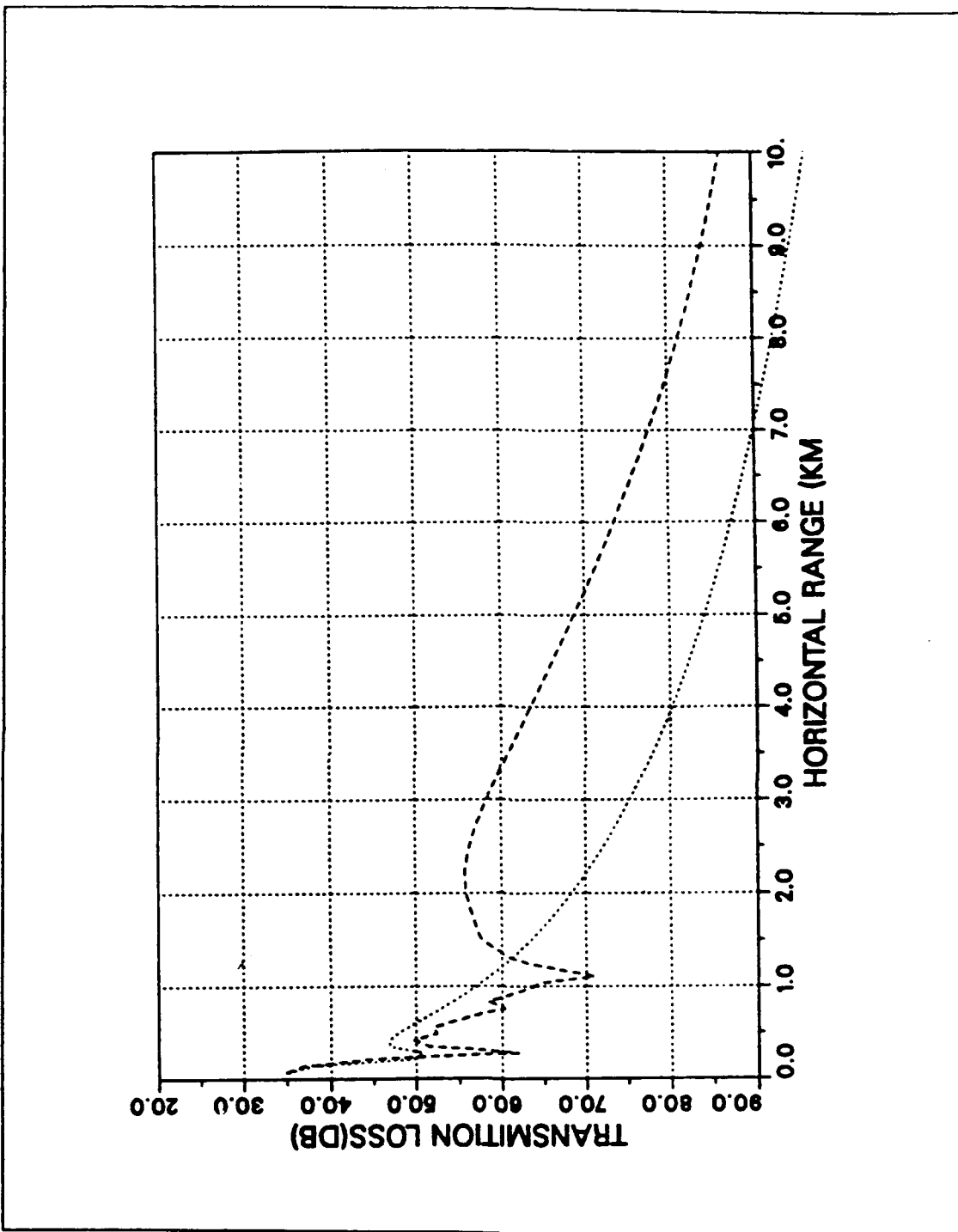


Figure 14. Downslope Transmission Loss (dB) vs Horizontal Source-Receiver Distance, to 10km, for  $\beta=10^\circ$ ,  $\gamma=5.0384^\circ$ ,  $\rho_1/\rho_2=0.9$ ,  $C_1/C_2=0.9$ .

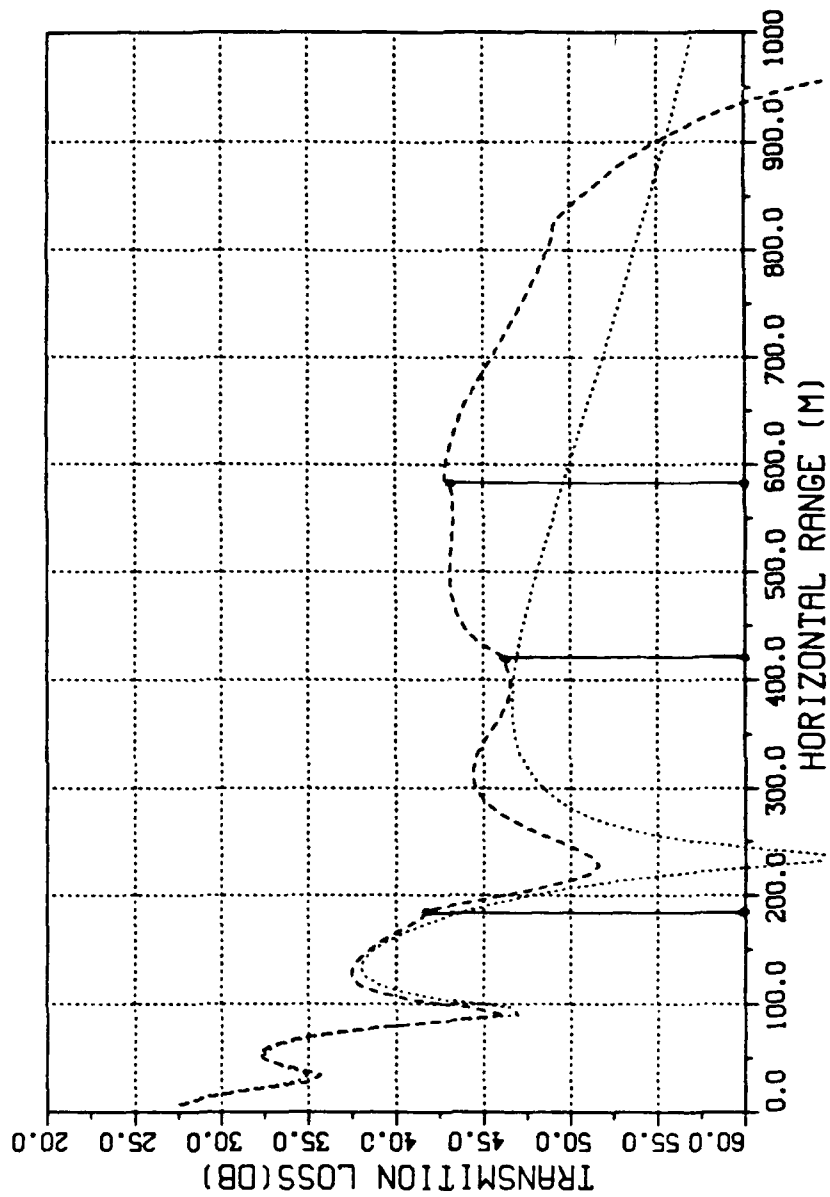


Figure 15. Downslope Transmission Loss (dB) vs Horizontal Source-Receiver Distance, to 1km, for  $\beta=5^\circ$ ,  $\gamma=2.5048^\circ$ ,  $\rho_1/\rho_2=0.9$ ,  $C_1/C_2=0.9$ .

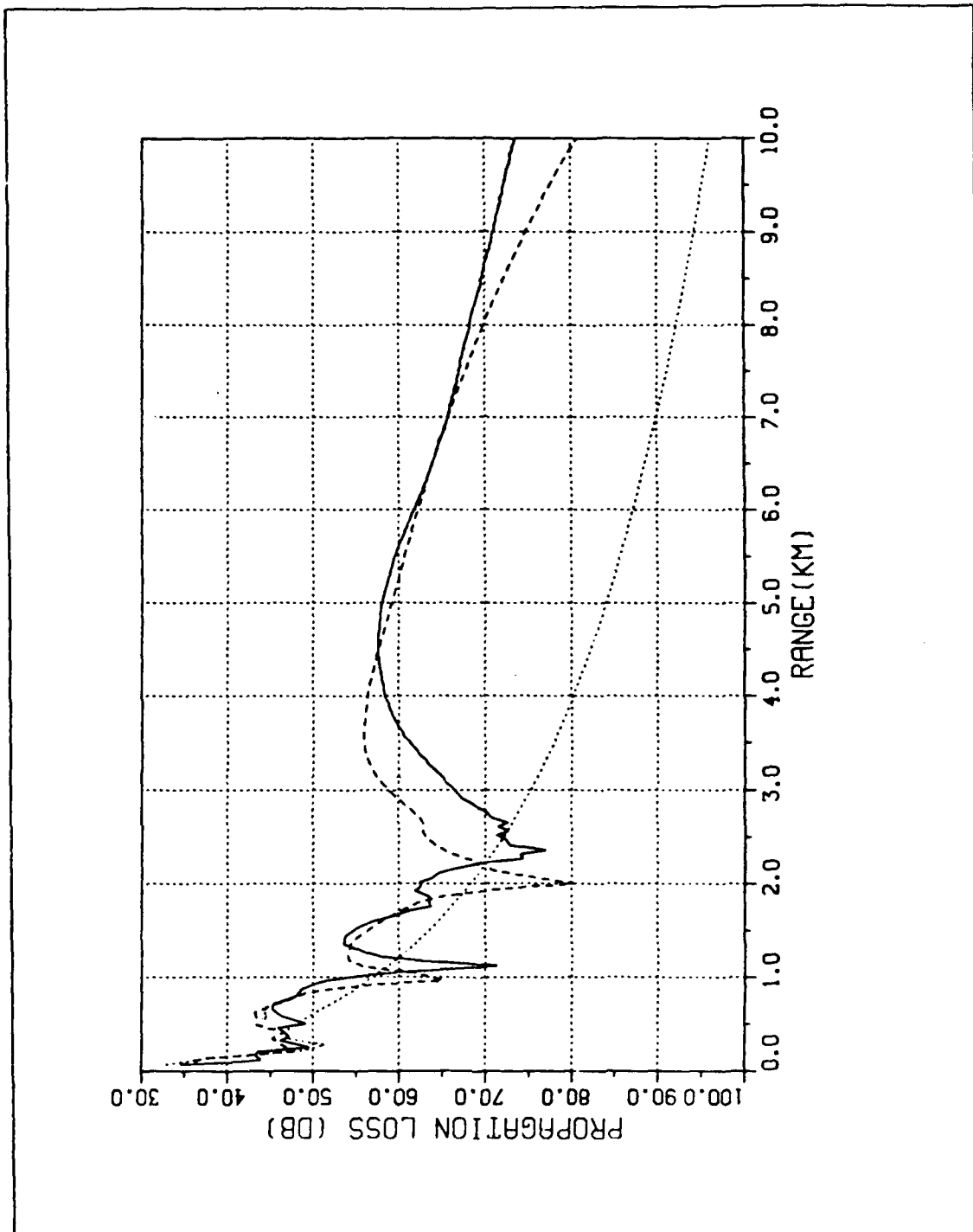


Figure 16. Downslope Transmission Loss (dB) vs Horizontal Source-Receiver Distance, to 10km, for  $\beta=5^\circ$ ,  $\gamma=2.4952^\circ$ ,  $\rho_1/\rho_2=0.9$ ,  $C_1/C_2=0.9$ .

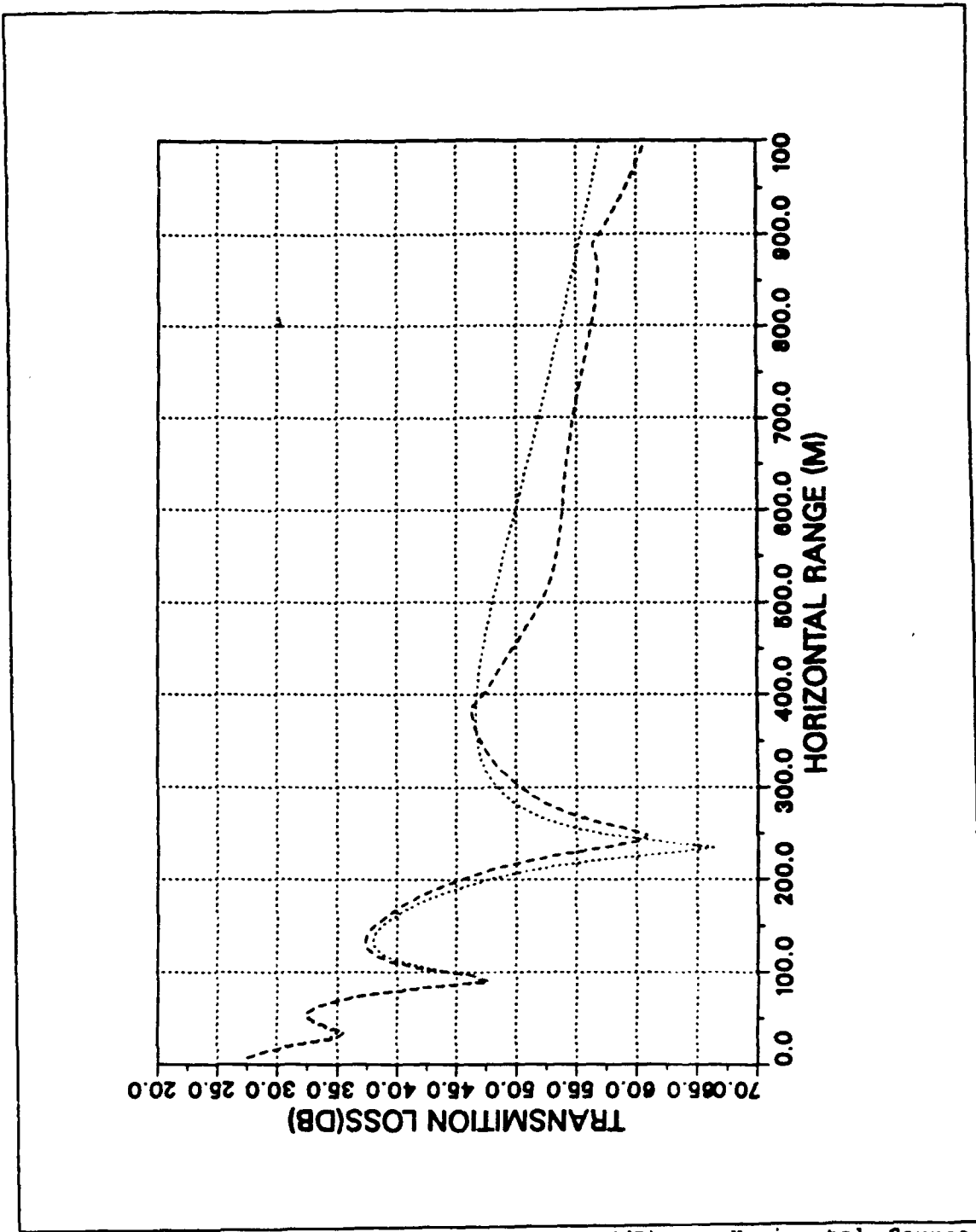


Figure 17. Downslope Transmission Loss (dB) vs Horizontal Source-Receiver Distance, to 1km, for  $\beta=10^\circ$ ,  $\gamma=5.0384^\circ$ ,  $\rho_1/\rho_2=0.94$ ,  $C_1/C_2=0.94$ .



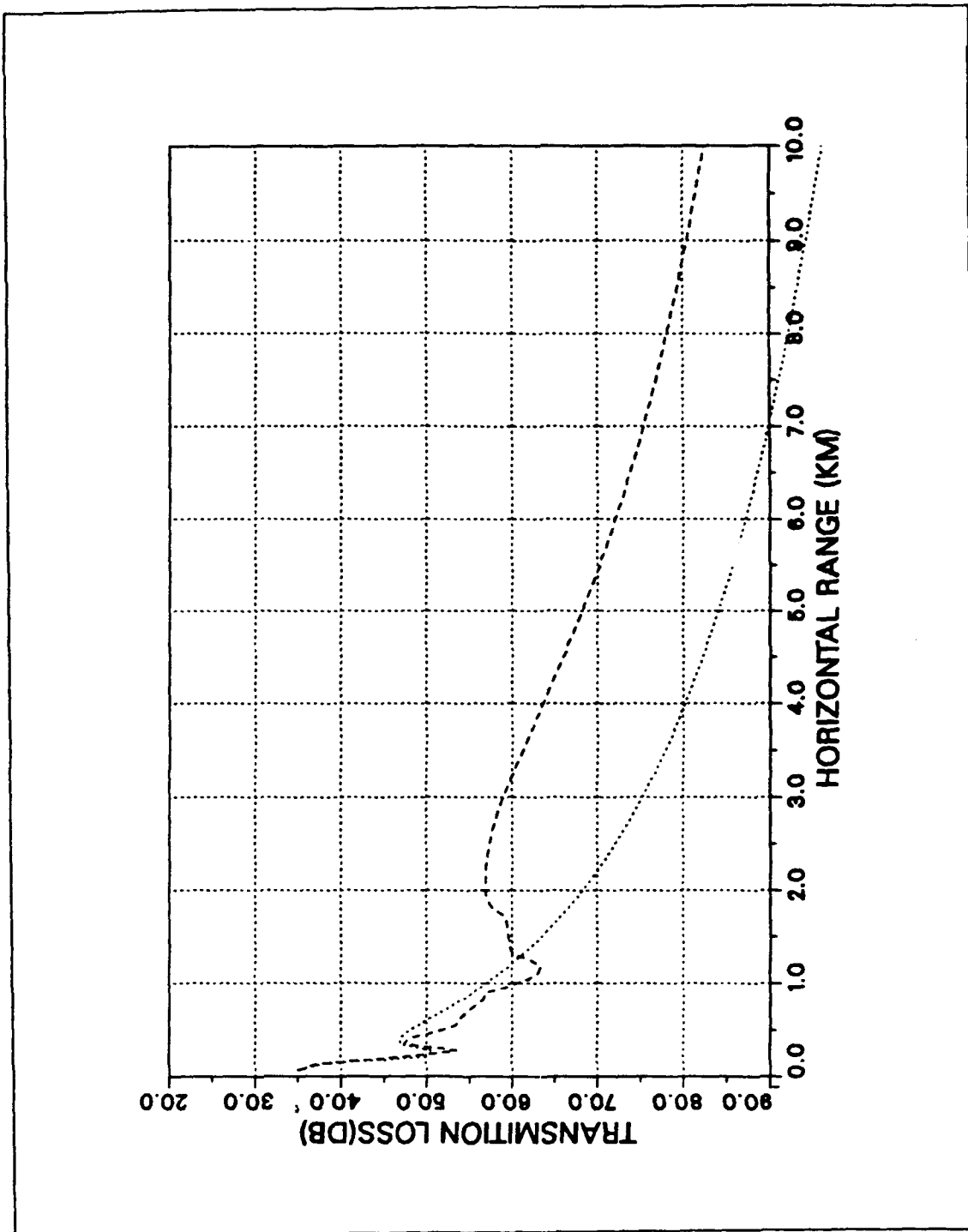


Figure 18. Downslope Transmission Loss (dB) vs Horizontal Source-Receiver Distance, to 10km, for  $\beta=10^\circ$ ,  $\gamma=5.0384^\circ$ ,  $\rho_1/\rho_2=0.94$ ,  $C_1/C_2=0.94$ .

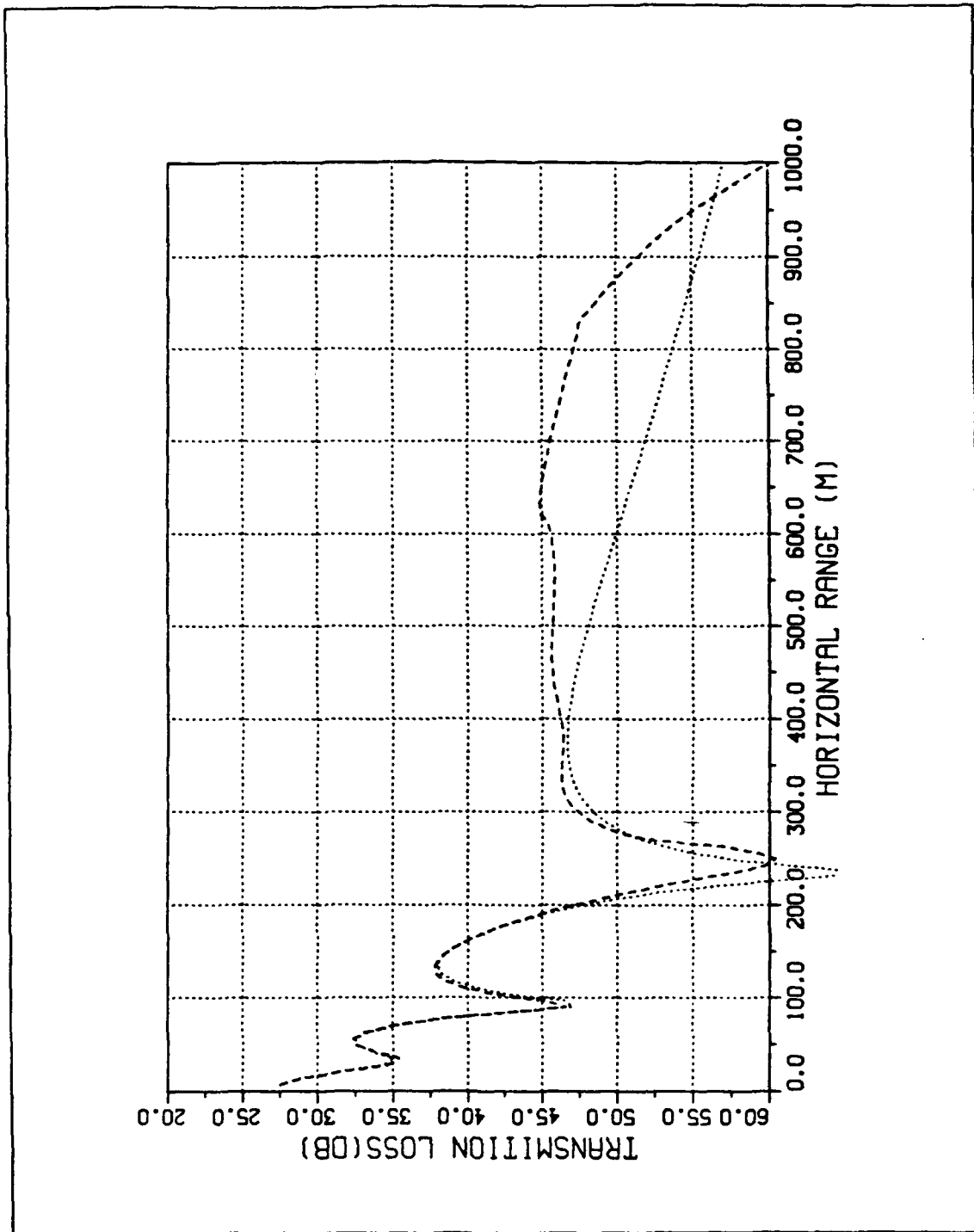


Figure 19. Downslope Transmission Loss (dB) vs Horizontal Source-Receiver Distance, to 1km, for  $\beta=5^\circ$ ,  $\gamma=2.5048^\circ$ ,  $\rho_1/\rho_2=0.94$ ,  $C_1/C_2=0.94$ .

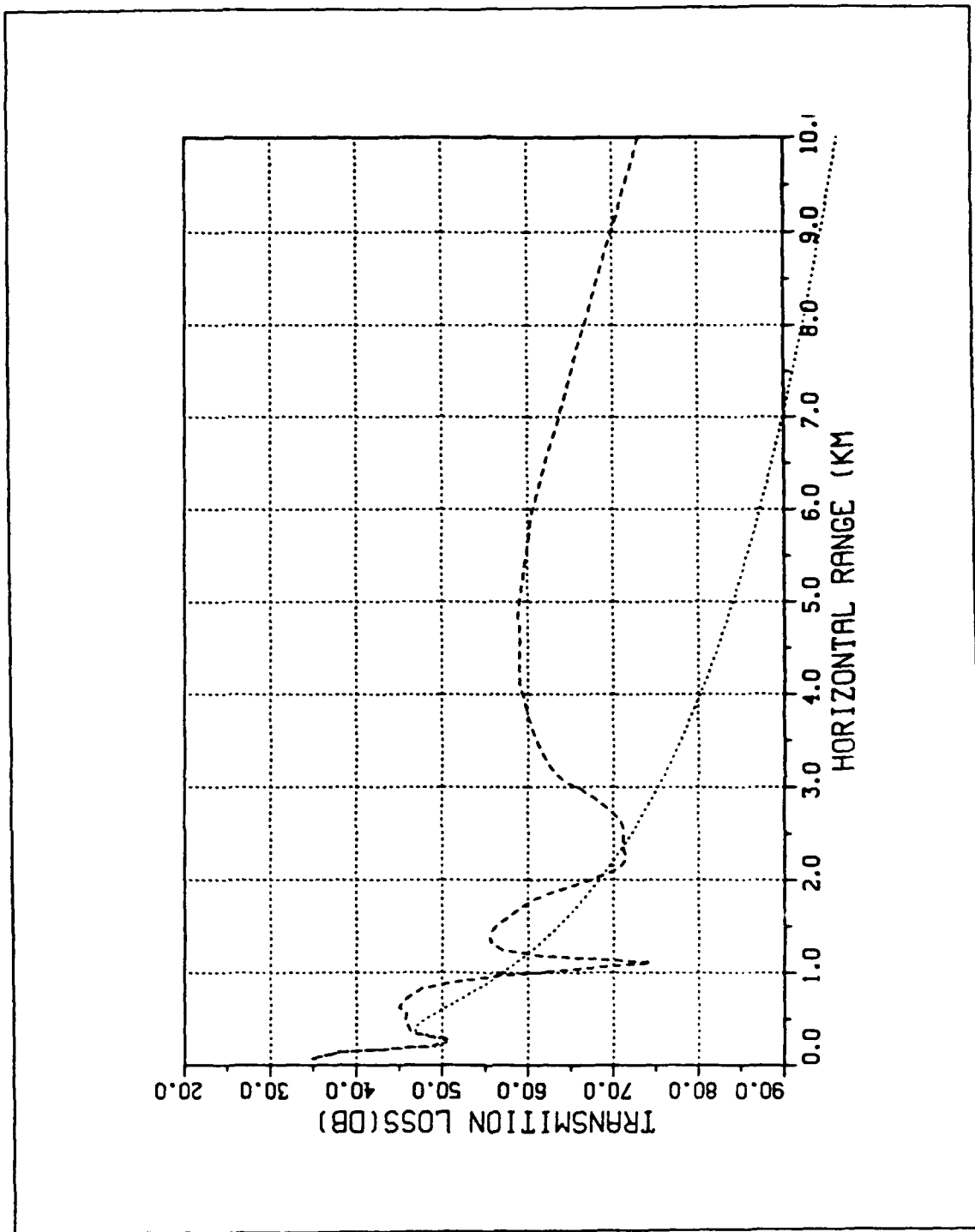


Figure 20. Downslope Transmission Loss (dB) vs Horizontal Source-Receiver Distance, to 10km, for  $\beta=5^\circ$ ,  $\gamma=2.5048^\circ$ ,  $\rho_1/\rho_2=0.94$ ,  $C_1/C_2=0.94$ .

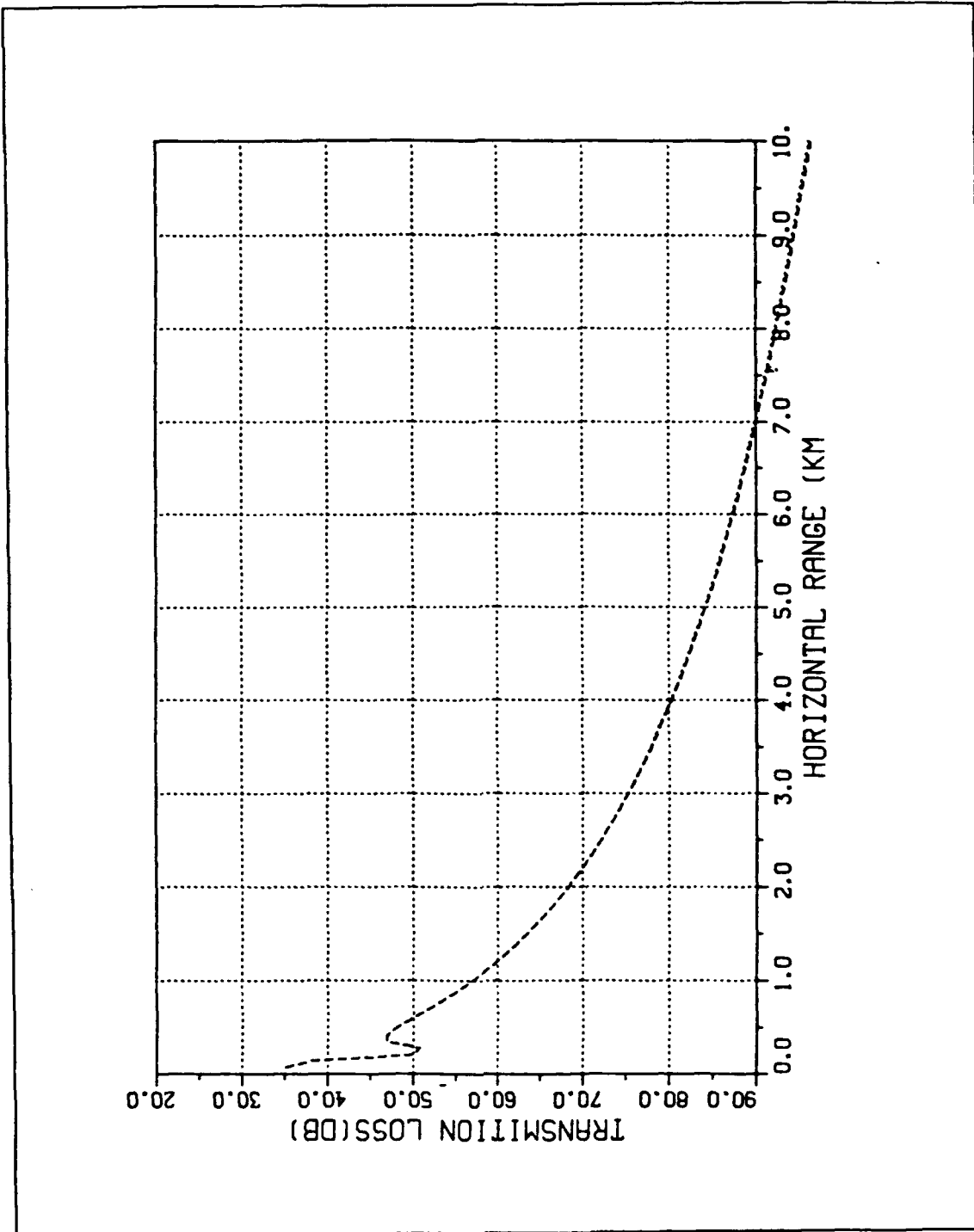


Figure 21. Downslope Transmission Loss (dB) vs Horizontal Source-Receiver Distance, to 10km, for  $\beta=10^\circ$ ,  $\gamma=5.0384^\circ$ ,  $\rho_1/\rho_2=0.9999$ ,  $C_1/C_2=0.9999$ .

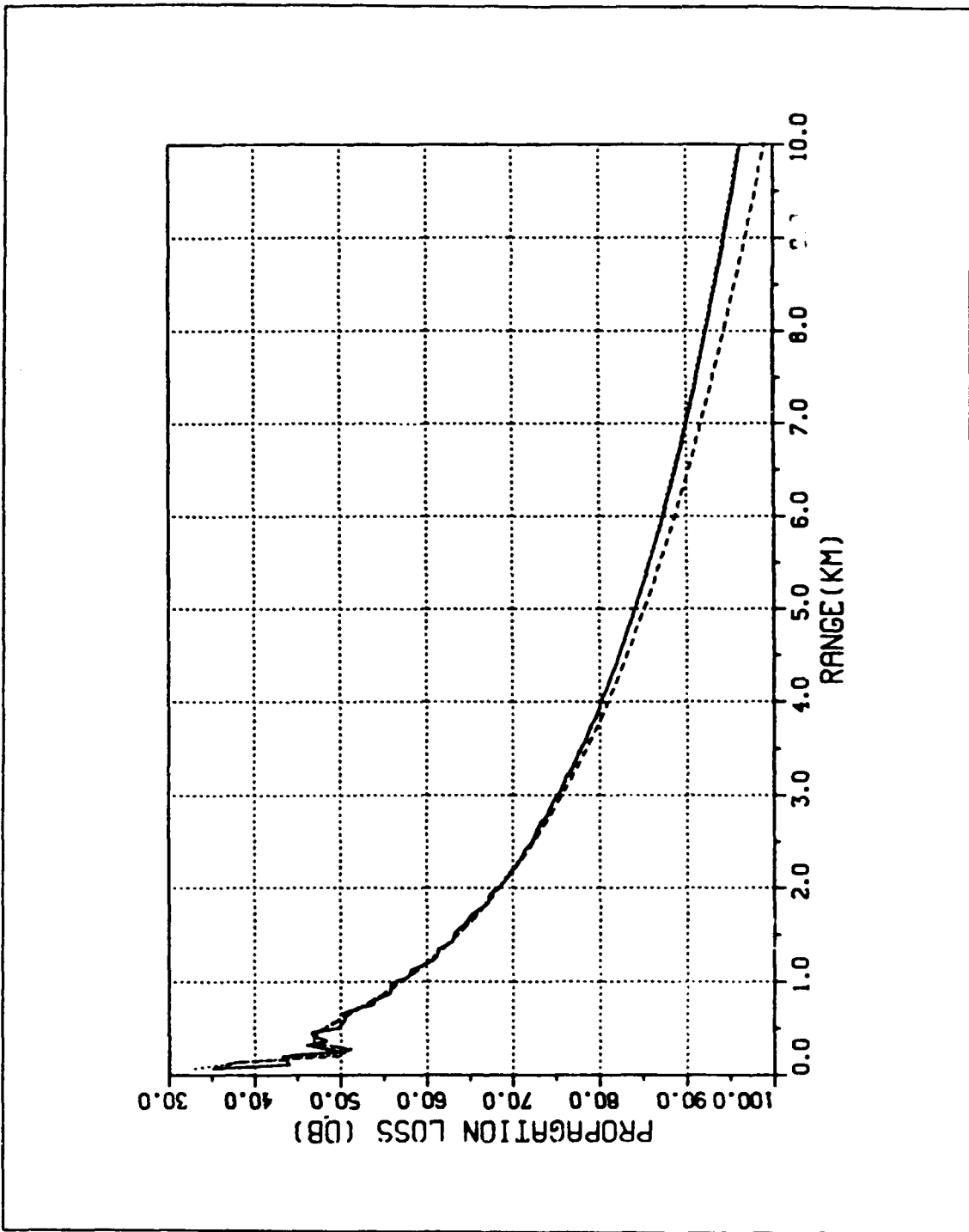


Figure 22. Downslope Transmission Loss (dB) vs Horizontal Source-Receiver Distance, to 10km, for  $\beta=5^\circ$ ,  $\gamma=2.4952^\circ$ ,  $\rho_1/\rho_2=0.9999$ ,  $C_1/C_2=0.9999$ .

## V. CONCLUSIONS AND RECOMMENDATIONS

Image theory is commonly accepted as a solution to the wedge-shaped ocean acoustic propagation problem, under the assumptions defined in sect. B of the development. Doublet analysis is a successful substitute for the image theory. This is important for two reasons:

1. It is a more compact solution.
2. The corresponding computer program execution time is faster than that of the image theory, because it requires fewer loops to calculate. Some tests which were done have shown that  $t_d \approx 0.55t_i$ , where  $t_d$  is the doublet analysis computer program execution time and  $t_i$  is the image theory analysis computer program execution time.

It is recommended that the doublet analysis be extended for the cross slope case, and that the corresponding computer program be extended for a fast bottom and to include absorption in the bottom.

It also appears possible an additional simplification, can be made according to the dipole approximation [Ref.8], where the doublet acoustic pressure without including any reflection coefficients

$$p(r, \theta, t) = -j \frac{2A}{r} \sin\left(\frac{1}{2} k_1 d \sin\theta\right) e^{j(\omega t - k_1 r)}$$

further reduces to

$$p(r, \theta, t) \doteq -j \frac{Ak_1 d}{r} \sin \theta e^{j(\omega t - k_1 r)}$$

when  $k_1 d = 2k_1 R_1 \gamma \ll 1$ . Using equations 1 and 4, this can also be expressed with respect to the scaling distance, as

$$\frac{R_1}{X_c} \frac{\pi \gamma}{\sin \theta_c \tan \beta} \ll 1$$

for a fast bottom, and

$$\frac{R_1}{X_s} \frac{\pi \gamma}{\tan \theta_s \tan \beta} \ll 1$$

for a slow bottom. It is obvious from the last two equations that the dipole approximation can be applied whenever  $R_1 \ll X$ .

APPENDIX "A"

NUMERICAL RESULTS OF COMPARISON BETWEEN THE IMAGE THEORY AND  
THE DOUBLET ANALYSIS

TABLE 1

Data for  $\beta=7^\circ$ ,  $\gamma=4^\circ$ ,  $R_1=4$ ,  $R_2=25$ ,  $\rho_1/\rho_2=0.7$ ,  $c_1=1500\text{m/s}$ ,  $c_2=1430\text{m/s}$

RECEIVER ANGLE	PRESSURE AMPLITUDE		PHASE ANGLE	
	IMAGE THEORY	DOUBLET ANALYSIS	IMAGE THEORY	DOUBLET ANALYSIS
0.07°	0.005314	0.005282	58.0°	85.4°
0.70°	0.055618	0.055174	56.9°	84.4°
1.40°	0.124116	0.123650	54.4°	81.8°
2.10°	0.212473	0.212157	51.3°	78.6°
2.80°	0.311260	0.311706	48.7°	75.8°
3.50°	0.394972	0.396090	46.8°	73.7°
4.20°	0.434343	0.435430	45.4°	72.3°
4.90°	0.412928	0.413046	44.1°	70.9°
5.60°	0.331062	0.329867	41.6°	68.3°
6.30°	0.200917	0.198261	33.5°	59.6°
7.00°	0.069522	0.072188	-25.4°	-4.0°



TABLE 2

Data for  $\beta=6^\circ$ ,  $\gamma=2^\circ$ ,  $R_1=0.8$ ,  $R_2=5$ ,  $\rho_1/\rho_2=0.8$ ,  $c_1=1500\text{m/s}$ ,  $c_2=1450\text{m/s}$

RECEIVER ANGLE	PRESSURE AMPLITUDE		PHASE ANGLE	
	IMAGE THEORY	DOUBLET ANALYSIS	IMAGE THEORY	DOUBLET ANALYSIS
0.06°	0.000372	0.000371	-50.2°	-46.0°
0.60°	0.003728	0.003667	-48.9°	-46.4°
1.20°	0.007214	0.007091	-49.9°	-47.6°
1.80°	0.010212	0.010050	-52.1°	-49.7°
2.40°	0.012559	0.012363	-55.3°	-53.0°
3.00°	0.014134	0.013921	-60.2°	-57.8°
3.60°	0.014946	0.014720	-67.1°	-64.7°
4.20°	0.015168	0.014929	-77.0°	-74.5°
4.80°	0.015224	0.014966	-90.5°	-88.1°
5.40°	0.015831	0.015523	-107.7°	-105.4°
6.00°	0.017739	0.017334	-126.1°	-123.9°

TABLE 3

Data for  $\beta=5^\circ$ ,  $\gamma=4^\circ$ ,  $R_1=2$ ,  $R_2=400$ ,  $\rho_1/\rho_2=0.6$ ,  $c_1=1500\text{m/s}$ ,  $c_2=1410\text{m/s}$

RECEIVER ANGLE	PRESSURE AMPLITUDE		PHASE ANGLE	
	IMAGE THEORY	DOUBLET ANALYSIS	IMAGE THEORY	DOUBLET ANALYSIS
0.05°	0.000087	0.000083	56.3°	78.8°
0.50°	0.000818	0.000817	62.6°	78.8°
1.00°	0.001532	0.001558	62.2°	78.9°
1.50°	0.002151	0.002158	63.0°	79.0°
2.00°	0.002537	0.002559	62.6°	79.2°
2.50°	0.002704	0.002725	63.3°	79.3°
3.00°	0.002639	0.002635	63.0°	79.4°
3.50°	0.002276	0.002292	62.4°	79.5°
4.00°	0.001699	0.001715	63.0°	79.4°
4.50°	0.000926	0.000942	60.5°	78.8°
5.00°	0.000025	0.000032	-30.6°	39.8°

TABLE 4

Data for  $\beta=4^\circ$ ,  $\gamma=1^\circ$ ,  $R_1=5$ ,  $R_2=12$ ,  $\rho_1/\rho_2=0.7$ ,  $c_1=1500\text{m/s}$ ,  $c_2=1420\text{m/s}$

RECEIVER ANGLE	PRESSURE AMPLITUDE		PHASE ANGLE	
	IMAGE THEORY	DOUBLET ANALYSIS	IMAGE THEORY	DOUBLET ANALYSIS
0.04°	0.040927	0.040984	-149.3°	-144.2°
0.40°	0.394236	0.394086	-148.6°	-143.5°
0.80°	0.701851	0.701115	-146.5°	-141.4°
1.20°	0.873027	0.871301	-142.3°	-137.3°
1.60°	0.915180	0.912006	-135.2°	-130.2°
2.00°	0.887048	0.882283	-124.6°	-119.6°
2.40°	0.851987	0.846756	-112.8°	-107.7°
2.80°	0.810276	0.805379	-104.5°	-99.4°
3.20°	0.704744	0.699685	-103.6°	-98.7°
3.60°	0.503485	0.498563	-115.2°	-110.9°
4.00°	0.315934	0.320342	-161.8°	-158.9°

TABLE 5

Data for  $\beta=3^\circ$ ,  $\gamma=1^\circ$ ,  $R_1=1$ ,  $R_2=10$ ,  $\rho_1/\rho_2=0.9$ ,  $c_1=1500\text{m/s}$ ,  $c_2=1475\text{m/s}$

RECEIVER ANGLE	PRESSURE AMPLITUDE		PHASE ANGLE	
	IMAGE THEORY	DOUBLET ANALYSIS	IMAGE THEORY	DOUBLET ANALYSIS
0.03°	0.000123	0.000127	-54.4°	-47.2°
0.30°	0.001255	0.001257	-49.8°	-47.2°
0.60°	0.002415	0.002414	-48.8°	-47.0°
0.90°	0.003352	0.003377	-49.4°	-46.6°
1.20°	0.004028	0.004066	-48.5°	-46.1°
1.50°	0.004384	0.004421	-47.5°	-45.1°
1.80°	0.004369	0.004409	-45.7°	-43.3°
2.10°	0.004010	0.004030	-42.1°	-40.2°
2.40°	0.003339	0.003329	-35.2°	-34.1°
2.70°	0.002471	0.002444	-20.8°	-20.1°
3.00°	0.001898	0.001799	12.7°	13.5°

APPENDIX "B"

\*\*\*\*\*

PROGRAM URTEXT

IMAGE THEORY--CROSS SLOPE PRESSURE VS RECEIVER ANGLE (D)

\*\*\*\*\*

```

INTEGER      I, I1, N, S1, S2, N1, A
REAL*4       B, CC, C2, D1, D2, G, PI, P1, P2, Q1, R1, R2, T, T4,
*           T6, Y0, Y1, Y2, Z1, Z2, Z3, Z4, Z5, Z6, T1(900),
*           R8(900), R9(900), S(900), C(900), E(900),
*           F(900), Z, R3, AL, PZ, D

```

```

DOUBLE PRECISION  Y, W0, W1

```

```

REAL            TQQ, TQQ1, TQQ2, TQQ3

```

```

PI =ACOS(-1.0D00)

```

```

WRITE(*,*) 'INPUT B, G, D1, CC, R1, R2, AL, Y0, A'

```

```

READ(6,*) B, G, D1, CC, R1, R2, AL, Y0, A

```

```

WRITE(6,2) B, G, D1, CC, R1, R2, AL, Y0, A

```

```

2  FORMAT('B = ',F4.1,/, 'G = ',F4.1,/, 'D1 = '
* ,F4.1,/, 'CC = ',F4.1,/, 'R1 = ',F4.1,/, 'R2 = ',F4.1,/, 'AL
* = ',F6.3,*/, 'Y0 = ',F4.1,/, 'A = ',I4)

```

C\*\*\*\*\*

C INPUT PARAMETERS

C\*\*\*\*\*

C B = WEDGE ANGLE (DEG)

C G = SOURCE ANGLE (DEG)

```

C      D = RECEIVER ANGLE (DEG)
C      N1= # OF IMAGE POINTS = INT(180/B)
C      R1 = SOURCE DISTANCE (IN DUMP DISTANCES) FROM APEX
C      R2 = RECEIVER DISTANCE (IN DUMP DISTANCES) FROM APEX
C      Y0 = DISTANCE (IN DUMP DISTANCES) ALONG APEX
C      D1 = RHO1/RHO2
C      CC = C1/C2
C      AL = ALPHA/K2
C      A  = # OF RECEIVER POSITIONS

```

```

C -----
C CHOOSE SLOW OR FAST BOTTOM BY VALUE OF SPEED RATIO
C CC = C1/C2 .
C -----

```

C\*\*\*\*\*

C MAIN PROGRAM

C\*\*\*\*\*

```

      N1 = INT(180./B)
      T6 = 180./PI
      B  = B/T6
      G  = B-(G/T6)
      C2 = CC**2
      TQQ = TAN(B)

```

```

C-----
C DECISION ABOUT SLOW OR FAST BOTTOM
C-----

```

```

C      T4 = PI/(2*SIN(ACOS(CC))*TAN(B)) FOR FAST BOTTOM
C      T4 = PI/(2*TAN(ACOS(1/CC))*TAN(B)) FOR SLOW BOTTOM

```

```

C-----

```

```

C

```

```

      IF (CC.LT.1) THEN

```

```

          TQQ1 =ACOS(CC)

```

```

          TQQ2 = SIN(TQQ1)

```

```

      ELSE

```

```

          TQQ1 = ACOS(1/CC)

```

```

          TQQ2 = TAN(TQQ1)

```

```

      ENDIF

```

```

      TQQ3 = 2.*TQQ2*TQQ

```

```

      T4   = PI/TQQ3

```

```

      Q1   = 1/DSQRT(2.0D00)

```

```

C

```

```

      DO 20  M1 = 1, A

```

```

          D = B-(B/A)*M1

```

```

          D2 = (Y0*Y0)+(R1*R1)+(R2*R2)

```

```

          R3 = 2.*R1*R2

```

```

          S1 = 1

```

```

C      |-----|

```

```

C      |THIS DO LOOP CALCULATES THE THETA(N)      |

```

```

C      |AND THE IMAGE SLANT RANGES R8(N) AND R9(N)|

```

```

C      |-----|

```

```

      DO 30  N = 1, N1

```

```

          IF(S1.GT.0) T1(N) = (N-1)*B+G

```

```

      IF(S1.LT.0) T1(N) = N*B-G
      S1 = - S1
      R8(N) = SQRT(D2-R3*COS(T1(N)-D))
      R9(N) = SQRT(D2-R3*COS(T1(N)+D))
30      CONTINUE
C      |-----|
C      |SUM THE PRESSURE OVER ALL IMAGES|
C      |-----|
      P1 = 0.0
      P2 = 0.0
      DO 40 N = 1, N1
          S2 = (-1)**(INT(N/2))
C      |-----|
C      |REFLECTION COEFFICIENTS ALONG NTH UPPER PATH|
C      |-----|
      W1 = 2*C2*AL
      I1 = INT((N-1)/2)
      DO 50 I = 1, I1
          S(I) = (R1*SIN(T1(N)-2*I*B)
&          +R2*SIN(2*I*B-D))/R8(N)
          IF(S(I).GE.1) S(I)=1
          C(I) = SQRT(1-(S(I)*S(I)))
          T = S(I)/D1
          W0 = (-C2+(C(I)*C(I)))
          Y = DSQRT((W0*W0)+(W1*W1))
          Z = W0

```



```

IF (Y.LE.Z) Y = Z
Y1 = Q1*SQRT(Y+W0)
Y2 = -Q1*SQRT(Y-W0)
Z1 = T-Y2
Z2 = -Y1
Z3 = Z1/(Z1*Z1+Z2*Z2)
Z4 = -Z2/(Z1*Z1+Z2*Z2)
Z1 = T+Y2
Z2 = Y1
Z5 = Z1*Z3-Z2*Z4
Z6 = Z1*Z4+Z2*Z3
E(I) = Z5
F(I) = Z6

```

```

50          CONTINUE

```

```

C|-----|

```

```

C          PRODUCT OF REFLECTION COEFFICIENTS ALONG NTH

```

```

C          UPPER PATH

```

```

C|-----|

```

```

Z1 = 0
Z2 = 0
Z3 = 0
Z4 = 0
Z5 = 1
Z6 = 0
IF(N.LE.2.00) GO TO 110
DO 60 I = 1, I1

```

```

        Z1 = E(I)
        Z2 = F(I)
        Z3 = Z5
        Z4 = Z6
        Z5 = Z1*Z3-Z2*Z4
        Z6 = Z1*Z4+Z2*Z3

60      CONTINUE
110     Z1 = Z5
        Z2 = Z6
        T  = T4*R8(N)
        Z3 = COS(T)
        Z4 = -SIN(T)
        Z5 = Z1*Z3-Z2*Z4
        Z6 = Z1*Z4+Z2*Z3
        P1 = P1+S2*Z5/R8(N)
        P2 = P2+S2*Z6/R8(N)
        I1=I1+1

C      |-----|
C      |REFLECTION COEFFICIENTS ALONG NTH LOWER PATH|
C      |-----|

        DO 70 I = 1, I1
            S(I) = (R1*SIN(T1(N)-2*(I-1)*B)
&                + R2*SIN(2*(I-1)*B+D))/R9(N)
            IF(S(I).GT.1) S(I)=1
            C(I) = SQRT(1-S(I)*S(I))
            T = S(I)/D1

```

```

W0 = -C2+C(I)*C(I)
Y = DSQRT((W0*W0)+(W1*W1))
Z = W0
IF(Y.LE.Z) Y = Z
Y1 = Q1*SQRT(Y+W0)
Y2 = -Q1*SQRT(Y-W0)
Z1 = T-Y2
Z2 = -Y1
Z3 = Z1/(Z1*Z1+Z2*Z2)
Z4 = - Z2/(Z1*Z1+Z2*Z2)
Z1 = T+Y2
Z2 = Y1
Z5 = Z1*Z3-Z2*Z4
Z6 = Z1*Z4+Z2*Z3
E(I) = Z5
F(I) = Z6

```

70

CONTINUE

```

C|-----|
C      PRODUCT OF REFLECTION COEFFICIENTS ALONG NTH LOWER
C      PATH
C|-----|

```

```

Z1 = 0
Z2 = 0
Z3 = 0
Z4 = 0
Z5 = 1

```

```

      Z6 = 0
      DO 80 I = 1, I1
          Z1 = E(I)
          Z2 = F(I)
          Z3 = Z5
          Z4 = Z6
          Z5 = Z1*Z3-Z2*Z4
          Z6 = Z1*Z4+Z2*Z3
80      CONTINUE
          Z1 = Z5
          Z2 = Z6
          T = T4*R9(N)
          Z3 = COS(T)
          Z4 = -SIN(T)
          Z5 = Z1*Z3-Z2*Z4
          Z6 = Z1*Z4+Z2*Z3
          P1 = P1+S2*Z5/R9(N)
          P2 = P2+S2*Z6/R9(N)
40      CONTINUE
          PZ = R1*SQRT(P1*P1+P2*P2)
          PH = ATAN2(P2,P1)*T6
          D = (B-D)*T6
          WRITE(6,3) D, PZ, PH
3      FORMAT(3X,'D = ',F8.4,3X,'PZ = ',F9.5,3X,'PH = ',F9.5)

```

20 CONTINUE

END

APPENDIX "C"

PROGRAM DOUBLT1C

C\*\*\*\*\*  
C THIS PROGRAM PRODUCES THE OUTPUTS OF THE DOUBLET ANALYSIS  
C OF THE IMAGE THEORY. THE SOURCE AND ITS FIRST SURFACE  
C REFLECTED IMAGE ARE TREATED AS A SEPARATE DOUBLET, AND  
C THE REST OF THE IMAGES ARE TREATED AS PAIRS OF ACOUSTIC  
C DOUBLETS. THIS PROGRAM IS INITIALLY MADE TO CALCULATE THE  
C REFLECTION COEFFICIENTS FOR A SLOW BOTTOM WITHOUT ANY  
C ABSORPTION IN THE BOTTOM. THAT WAY, THE REFLECTION  
C COEFFICIENTS ARE REAL, AND THE PROGRAM IS SIMPLER TO  
C INITIALLY VERIFY THE VALIDITY OF THIS NEW ANALYSIS. IT  
C ALSO WORKS FOR DOWNSLOPE/UPSLOPE CASE ONLY. THE INITIAL  
C SETUP (BEFORE REACHING THE DOLOOP # 20) IS APPLICABLE TO  
C ALL OTHER CASES (CROSS SLOPE, FAST BOTTOM, ABSORPTION IN  
C THE BOTTOM), BUT THE PROGRAM WOULD REQUIRE MODIFICATIONS  
C IN DOLOOP #20 AND BEYOND

C\*\*\*\*\*

INTEGER A, N1, NQ1, M1, K, M, MQ, N  
DOUBLE PRECISION B, G, D1, C1, C2, Y0, R1, R2, R3, CC, PI, D2,  
\*TQQ, TQQ1, PQ2 (5000), TQQ2, TQQ3, T4, T6, R0P, SNS0P, P1, P2,  
\*Z1 (90), Z2 (90), GNP (90), THP (90), EP (90), PHIP (90),  
\*PSIP (90), Z3 (90), Z4 (90), T11 (90), RL (90), RU (90), SL, SU,  
\*RLD (90), RUD (90), DRU (90), DRL (90), SUMRU (90), SUMRL (90),

```

*Z5(90),Z6(90),Z7(90),Z8(90),RN0P(90),D(5000),PQ1(5000)
PI = ACOS(-1.0D00)
WRITE(*,*)'INPUT B,G,R1,R2,Y0,D1,C1,C2,A'
READ(5,*)B,G,R1,R2,Y0,D1,C1,C2,A
WRITE(6,2)B,G,R1,R2,Y0,D1,C1,C2,A
2  FORMAT(9X,'B = ',F5.2,/, 6X,'G = ',F6.2,/, 6X,'R1 =
*',F5.2,/, 6X,'R2 = ',F5.2,/, 6X,'Y0 = ',F3.1,/,
*6X,'D1 = ',F4.2,/, 6X,'C1 = ',F7.2,/, 6X,'C2 =
*',F10.4,/, 6X,/,9X,'A = ',I4)
C*****
C  *INPUT PARAMETERS
C*****
C  FR  = FREQUENCY
C  X   = SCALING DISTANCE
C  B   = WEDGE ANGLE (DEG)
C  G   = SOURCE ANGLE MEASURED FROM THE SURFACE (DEG)
C  D   = RECEIVER ANGLE MEASURED FROM THE SURFACE (DEG)
C  N1  = NUMBER OF MONOPOLES (IMAGE POINTS)
C  NQ1 = NUMBER OF PAIRS OF ACOUSTIC DOUBLETS
C  R1  = SOURCE DISTANCE (IN DUMP DISTANCES) FROM APEX
C  R2  = RECEIVER DISTANCE (IN DUMP DISTANCES) FROM APEX
C  Y0  = SOURCE-RECEIVER HORIZONTAL DISTANCE IN DUMP
C      DISTANCES ALONG APEX
C  D1  = RHO1/RHO2
C  CC  = C1/C2
C  A   = NUMBER OF RECEIVER POSITIONS

```

```

C*****
C      CHOOSE SLOW OR FAST BOTTOM BY VALUE OF SPEED RATIO
C      CC = C1/C2
C*****
C*****
C              M A I N      P R O G R A M
C*****

      K = 0
      CC = C1/C2
      N1 = INT(180./B)
      NQ1 = INT((INT(360./B)-2)/4)
      T6 = 180./PI
      B = B/T6
      G = G/T6
      D2 = 1./D1
      TQQ = TAN(B)

C
C *****
C      DECISION ABOUT SLOW OR FAST BOTTOM
C      T4 = PI/(2*SIN(ACOS(CC))*TAN(B)) FOR FAST BOTTOM
C      T4 = PI/(2*TAN(ACOS(1/CC))*TAN(B)) FOR SLOW BOTTOM
C *****
      IF(CC.LT.1) THEN
          TQQ1 = ACOS(CC)
          TQQ2 = SIN(TQQ1)
      ELSE

```



```

      TQQ1 = ACOS (1/CC)
      TQQ2 = TAN (TQQ1)

ENDIF

TQQ3 = 2.*TQQ2*TQQ
T4 = PI/TQQ3
PRINT*, 'K1X = ', T4
C   X = T4*C1/(2*PI*FR)

      CALL EXCMS ('FILEDEF 79 CLEAR')

DATA NOA/79/

      CALL EXCMS ('FILEDEF 79 DISK IFDOUT4 PLOTTER A1')

R3 = 2*R1*R2
DO 20  M1 = 1,A
      K = K+1
C   START COUNTING THE RECEIVERS POSITIONS

      D (M1) = (B/A)*M1

DO N = 1,N1
C   CALCULATION OF THE ANGLE OF EACH IMAGE FROM THE BOTTOM

      IF ((N/2) .LT. (N/2.)) THEN

          T11 (N) = N*B-G

          ELSE

          T11 (N) = (N-1)*B+G

      ENDIF
C   CALCULATION OF THE IMAGE SLANT RANGES
C   LOWER IMAGES

      RLD (N) = DSQRT (R1**2+R2**2+Y0**2-
&
          -R3*COS (T11 (N) +B-D (M1) ))

```

C UPPER IMAGES

```
RUD(N) = DSQRT(R1**2+R2**2+Y0**2-  
& -R3*COS(T11(N)-B+D(M1)))
```

ENDDO

C CALCULATION OF THE REFLECTION COEFFICIENTS FOR A SLOW  
BOTTOM WITHOUT ANY ABSORPTION

C LOWER IMAGES

```
DO N = 1,N1
```

```
RL(N) = 1.
```

```
MQ = INT((N-1)/2)
```

```
DO M = 0,MQ
```

```
SK1 = R2*DSIN((2*M+1)*B-D(M1))
```

```
SL = DASIN((R1*DSIN(T11(N)-2*M*B)+SK1)/RLD(N))
```

```
A50 = DSQRT(CC**2-(COS(SL))**2)
```

```
VL = (D2*DSIN(SL)-A50)/(D2*DSIN(SL)+A50)
```

```
RL(N) = RL(N)*VL
```

ENDDO

ENDDO

C UPPER IMAGES

```
DO N = 3,N1
```

C THIS DOLOOP STARTS FROM THE THIRD UPPER IMAGE BECAUSE THE

C FIRST AND THE SECOND UPPER IMAGES ARE CONSIDERED AS A

C NEUTRAL DOUBLET

```
RU(N) = 1.
```

```
MQ = INT((N-1)/2)
```

```
DO M = 1,MQ
```

```

SK2 = R2*DSIN((2*M-1)*B+D(M1))
SU = DASIN((R1*DSIN(T11(N)-2*M*B)+SK2)/RUD(N))
B50 = DSQRT(CC**2-(COS(SU))**2)
VU = (D2*DSIN(SU)-B50)/(D2*DSIN(SU)+B50)
RU(N) = RU(N)*VU
ENDDO
ENDDO
C   SUM AND DIFFERENCE OF THE REFLECTION COEFFICIENTS
C   BETWEEN THE TWO IMAGES OF EACH ACOUSTIC DOUBLET
DO N = 1,NQ1
  IF ((2*(N+2)).LE.N1) THEN
    DRU(N) = RU(2*N+1)-RU(2*N+2)
    SUMRU(N) = RU(2*N+1)+RU(2*N+2)
    DRL(N) = RL(2*N-1)-RL(2*N)
    SUMRL(N) = RL(2*N-1)+RL(2*N)
  ELSE
    DRU(N) = 0
    SUMRU(N) = 0
    DRL(N) = 0
    SUMRL(N) = 0
  ENDIF
ENDDO
C   PRESSURE FIELD FROM THE NEUTRAL DOUBLET (EQ.31)
R0P = SQRT(R1**2+R2**2+Y0**2-2*R1*R2*COS(D(M1)))
SNS0P = (R2/R0P)*D(M1)
P1 = (2/R0P)*SIN(T4*R1*G*SNS0P)*(SIN(T4*R0P))

```

```

P2 = (2/R0P)*SIN(T4*R1*G*SNS0P)*(COS(T4*R0P))
C      CALCULATION OF THE TOTAL PRESSURE FIELD. ADD THE
C      FIELD OVER ALL DOUBLETS ACCORDING TO EQS.51 AND 52
DO 30  N = 1,NQ1
C      EQ.35
      RN0P(N) = SQRT(R1**2+R2**2+Y0**2-
&          -2*R1*R2*COS(2*N*B))
C      EQ.45
      GNP(N) = T4*R1*R2/RN0P(N)
C      EQ.46
      THP(N) = GNP(N)*G*SIN(2*N*B)
C      EQ.48
      EP(N) = GNP(N)*G*D(M1)*COS(2*N*B)
C      EQ.47
      PHIP(N) = GNP(N)*D(M1)*SIN(2*N*B)
C      EQ.49
      KSIP(N) = 0.5*(D(M1)*EP(N)/G-
&          -PHIP(N)**2/(T4*RN0P(N)))
C      APPLY EQ 52
      Z1(N) = SIN(THP(N)+EP(N))*
&          *SIN(T4*RN0P(N)+PHIP(N)+KSIP(N))
      Z1(N) = SUMRU(N)*Z1(N)
      Z2(N) = COS(THP(N)+EP(N))*
&          *COS(T4*RN0P(N)+PHIP(N)+KSIP(N))
      Z2(N) = DRU(N)*Z2(N)
      Z3(N) = SIN(THP(N)-EP(N))*

```

```

&          *SIN (T4*RN0P (N) -PHIP (N) +KSIP (N) )
Z3 (N) = -SUMRL (N) *Z3 (N)
Z4 (N) = COS (THP (N) -EP (N) ) *
&          *COS (T4*RN0P (N) -PHIP (N) +KSIP (N) )
Z4 (N) = -DRL (N) *Z4 (N)
Z5 (N) = SIN (THP (N) +EP (N) ) *
&          *COS (T4*RN0P (N) +PHIP (N) +KSIP (N) )
Z5 (N) = SUMRU (N) *Z5 (N)
Z6 (N) = COS (THP (N) +EP (N) ) *
&          *SIN (T4*RN0P (N) +PHIP (N) +KSIP (N) )
Z6 (N) = -DRU (N) *Z6 (N)
Z7 (N) = COS (THP (N) -EP (N) ) *
&          *SIN (T4*RN0P (N) -PHIP (N) +KSIP (N) )
Z7 (N) = DRL (N) *Z7 (N)
Z8 (N) = SIN (THP (N) -EP (N) )
&          *COS (T4*RN0P (N) -PHIP (N) +KSIP (N) )
Z8 (N) = -SUMRL (N) *Z8 (N)
P1 = (-1)**N*(1./RN0P (N) ) *
&          * (Z1 (N) +Z2 (N) +Z3 (N) +Z4 (N) ) +P1
P2 = (-1)**N*(1./RN0P (N) ) *
&          * (Z5 (N) +Z6 (N) +Z7 (N) +Z8 (N) ) +P2
30  CONTINUE
C    AMPLITUDE
PQ1 (M1) = R1*SQRT (P1**2+P2**2)
C    PHASE
PQ2 (M1) = ATAN2 (P2,P1) *T6

```

```

C      CONVERT THE RECEIVER ANGLE IN DEGREES
      D (M1) = D (M1) *180./PI
C      WRITE (6, 3) D (M1) , PQ1 (M1) , PQ2 (M1)
C 3    FORMAT (9X, F6.3, 8X, F9.6, 8X, F10.5)
      20  CONTINUE
C      STORE THE RESULTS IN THE FILE IFDOUT4 PLOTTER A1. FROM
C      THAT FILE THEY ARE RECALLED IN URTEXT1C EXECUTION, FOR
C      COMPARISON WITH THE IMAGE THEORY RESULTS.
      DO 21 J = 1, K
          WRITE (NOA, *) D (J) , PQ1 (J) , PQ2 (J)
      21  CONTINUE
      END

```

## LIST OF REFERENCES

1. Jensen, F.B., and Tindle, C.T., *Numerical Modeling Results for Mode propagation in a Wedge*, J.A.S.A., v.82(1), pp.211-216, July 1987.
2. Jaeger, L.E., *A Computer Program for Solving the Parabolic Equation Using an Implicit Finite-Difference Solution Method Incorporating Exact Interface Conditions*, Master's Thesis, Naval Postgraduate School, Monterey, California, 1983.
3. Naval Postgraduate School Report 61-79-002, *Programs for the evaluation of the Acoustic Pressure Amplitude and Phase at the bottom of a Wedge-Shaped Fluid Layer Overlaying a Fast Fluid Half Space*, by Coppens, A.B., Sanders, J.V., Ioannou, I., and Kawamura, W., December 1978.
4. Baek, C.K., *The Acoustic Pressure in a Wedge-Shaped Water Layer Overlying a Fast Fluid Bottom*, Master's Thesis, Naval Postgraduate School, Monterey, California, March 1984.
5. Lesesne, P.K., *Development of Computer Programs Using the Method of Images to Predict the Sound Field in a Wedge Overlying a Fast Fluid and Comparison with Laboratory Experiments*, Master's Thesis, Naval Postgraduate School, Monterey, California, December 1984.
6. Paliatsos, D., *Computer Studies of Sound Propagation in a Wedge-Shaped Ocean with Penetrable Bottom*, Master's Thesis, Naval Postgraduate School, Monterey, California, March 1989.
7. Jong Rok, K., *Comparison of Sound Pressure in a Wedge-Shaped Ocean as predicted by an Image Method and a PE Model*, Master's Thesis, Naval Postgraduate School, Monterey, California, December 1990.
8. Coppens, A.B., Sanders, J.V., Frey, A.R., and Kinsler, L.E., *Fundamentals of Acoustics*, third edition, pp.169-170, Monterey, California, January 1980.
9. Personal Communication with A.B.Coppens and J.V.Sanders. Naval Postgraduate School, Monterey, CA 93940, December 1991.

### INITIAL DISTRIBUTION LIST

1. Defence Technical Information Center 2  
Cameron Station  
Alexandria, VA 22304-6145
2. Library, Code 52 2  
Naval Postgraduate School  
Monterey, CA 93943-5002
3. Department Library, Code PH 2  
Department of Physics and Chemistry  
Naval Postgraduate School  
Monterey, CA 93943-5002
4. Dr. A.B.Coppens, Code PH/Cz 2  
Department of Physics and Chemistry  
Naval Postgraduate School  
Monterey, CA 93943-5002
5. Dr. J.V.Sanders, Code PH/Sd 2  
Department of Physics and Chemistry  
Naval Postgraduate School  
Monterey, CA 93943-5002
6. Embassy of Greece 1  
Naval Attache  
2228 Massachusetts Av., N.W.  
Washington D.C. 20008
7. Hellenic Navy General Staff 4  
Second Branch, Education Department  
Stratopedon Papagou  
Athens, Greece
8. George Nassopoulos 1  
98A Anatolis st.  
Papagos, 15669  
Athens, Greece